1   **Facial shape and allometry quantitative trait locus intervals in the Diversity Outbred mouse**

2   **are enriched for known skeletal and facial development genes**

3   **Authors**

4   David C. Katz[1*], J. David Aponte[1], Wei Liu[1], Rebecca M. Green[1], Jessica M. Mayeux[2], K. Michael

5   Pollard[2], Daniel Pomp[3], Steven C. Munger[4], Steven A. Murray[4], Charles C. Roseman[5],

6   Christopher J. Percival[6], James Cheverud[7], Ralph S. Marcucio[8], Benedikt Hallgrímsson[1*]

7   **Affiliations**

8   [1] Department of Cell Biology & Anatomy, Alberta Children's Hospital Research Institute and

9   McCaig Bone and Joint Institute, Cumming School of Medicine, University of Calgary, AB,

10 Canada

11 [2] Department of Molecular Medicine, The Scripps Research Institute, La Jolla, CA, USA

12 [3] Department of Genetics, University of North Carolina Medical School, Chapel Hill, NC, USA

13 [4] The Jackson Laboratory, Bar Harbor, ME, USA

14 [5] Department of Animal Biology, University of Illinois Urbana Champaign, Urbana, IL, USA

15 [6] Department of Anthropology, Stony Brook University, Stony Brook, NY, USA

16 [7] Department of Biology, Loyola University Chicago, Chicago, IL, USA

17 [8] Department of Orthopaedic Surgery, School of Medicine, University of California San

18 Francisco, San Francisco, CA, USA

19 *** Corresponding authors**

20 bhallgri@ucalgary.ca, david.katz@ucalgary.ca

21

Abstract

The biology of how faces are built and come to differ from one another is complex. Discovering the genes that contribute to differences in facial morphology is one key to untangling this complexity, with important implications for medicine and evolutionary biology. This study maps quantitative trait loci (QTL) for skeletal facial shape using Diversity Outbred (DO) mice. The DO is a randomly outcrossed population with high heterozygosity that captures the allelic diversity of eight inbred mouse lines from three subspecies. The study uses a sample of 1147 DO animals (the largest sample yet employed for a shape QTL study in mouse), each characterized by 22 three-dimensional landmarks, 56,885 autosomal and X-chromosome markers, and sex and age classifiers. We identified 37 facial shape QTL across 20 shape principal components (PCs) using a mixed effects regression that accounts for kinship among observations. The QTL include some previously identified intervals as well as new regions that expand the list of potential targets for future experimental study. Three QTL characterized shape associations with size (allometry). Median support interval size was 3.5 Mb. Narrowing additional analysis to QTL for the five largest magnitude shape PCs, we found significant overrepresentation of genes with known roles in growth, skeletal development, and sensory organ development. For most intervals, one or more of these genes lies within 0.25 Mb of the QTL's peak. QTL effect sizes were small, with none explaining more than 0.5% of facial shape variation. Thus, our results are consistent with a model of facial diversity that is influenced by key genes in skeletal and facial development and, simultaneously, is highly polygenic.

Author Summary

44   The mammalian face is a complex structure serving many functions. We studied the

45   genetic basis for facial skeletal diversity in a large sample of mice from an experimental

46   population designed for the study of complex traits. We quantified the contribution of genetic

47   variation to variation in three-dimensional facial shape across more than 55,000 genetic

48   markers spread throughout the mouse genome. We found 37 genetic regions which are very

49   likely to contribute to differences in facial shape. We then conducted a more detailed analysis

50   of the genetic regions associated with the most variable aspects of facial shape. For these

51   regions, a disproportionately large number of genes are known to be important to growth and

52   to skeletal and facial development. The magnitude of these genetic contributions to differences

53   in facial shape are consistently small. Our results therefore support the notion that facial

54   skeletal diversity is influenced by many genes of small effect, but that some of these small

55   effects may be related to genes that are fundamental to skeletal and facial development.

56

Introduction

57

58   The facial skeleton is a complex morphology that serves a diverse set of critical roles. It

59   houses and protects the forebrain and most sensory organs and provides essential anatomy for

60   oral communication, feeding, and facial expression. Structured differences (covariance) in facial

61   shape and form depend upon variation in the biological processes that coordinate facial

62   development [1-7]. Understanding how these processes act and combine to build a facial

63   skeleton requires interrogation at multiple levels of the genotype-phenotype (GP) map [8, 9].

64   Among the most fundamental of these inquiries is the search for genetic variants that

65   contribute to facial variation. These genetic variants are the basic building blocks of diversity

66   and, within species, circumscribe the potential for short-term evolutionary change [10, 11].

67   Over the past decade, dozens of studies in humans, mouse models, and other species have

68   dissected GP associations for the craniofacial complex using moderate-to-high density genetic

69   maps (tens of thousands to millions of markers). The focus is typically on additive effects [12],

70   though some recent work considers interactions among loci [4, 13, 14].

71   In humans, genome-wide association studies (GWAS) targeting variation in soft tissue

72   facial form have been completed for European [15-20], African [21], South American [22], and

73   Asian [23] cohorts. Collectively, the studies report around 50 loci for facial morphology [24].

74   While there is limited overlap in the candidate gene sets among studies [25], and though many

75   of the individual genes have no previously known role in facial development [3], the genes that

76   do replicate across GWAS (*PAX 1*, *PAX3, HOXD* cluster genes, *DCHS2*, *SOX9*) are known to be

77   important to facial and/or skeletal morphogenesis.

78   Compared to human studies, mapping the genetics of facial variation in mice offers

79   several benefits, including greater control over genetic and environmental variation and the

80   ability to record observations, directly or *in silico*, on the skeleton itself [14, 26-31]. In recent

81   years, the focus of mouse skull QTL analyses has expanded to include tests of enrichment for

82   disease phenotypes and roles in skull development, as well as the search for and validation of

83   candidate genes [32-34]. Dozens of QTL have been identified. As with human facial shape

84   GWAS candidates, this is encouraging but also a small beginning—on the order of the total

85   number of loci identified for human height just a decade ago [35]. Quantitative genetics

86   analyses [32, 36, 37] and expression and epigenomic atlases of facial development both

87   strongly point to the potential for hundreds or thousands of genetic loci with as-yet-undetected

4

88   QTL variance contributions [38-40]. Increased sample sizes, greater mapping resolution, and the

89   development of new experimental lines all have the potential to expand the facial shape QTL

90   library and increase the precision of variant localization [41-43].

91   The present study maps mouse facial shape QTL in what is, to date, the largest sample

92   yet used for this purpose (n = 1147). We use Diversity Outbred mice (DO; Jackson Laboratory,

93   Bar Harbor, ME), a random outcross model derived from the Collaborative Cross (CC) founding

94   lines [43-46]. The DO is specifically designed for genetic mapping of complex traits. Each

95   animal's genome is a unique mosaic of the genetic diversity present in the CC founders—more

96   than 45 million segregating SNPs [47]. Random outcrossing (of non-sibs) over many DO

97   generations maintains this diversity and increases recombination frequency, which is critical for

98   reducing confidence intervals of localized QTL [41]. Compared to classic backcross and

99   intercross designs, the combinatorial possibilities for allelic variation within and among DO

100 animals are vast. The genetic diversity in a DO sample may thus mimic diversity in the natural

101 populations that animal models are meant to illuminate.

102   We quantify facial shape with 22 three-dimensional landmarks **(Fig 1)** and estimate its

103 association with founder haplotype variation at 56,885 genetic markers. The dependent

104 observations in the QTL scans are scores on shape PCs. For each PC explaining more than 1% of

105 shape variation, we identify statistically significant marker effects using a mixed effects

106 regression model that simultaneously accounts for kinship among animals [48, 49]. We then

107 undertake a more detailed analysis of QTL intervals for shape PCs 1-5. We estimate founder

108 coefficients, test whether the overall gene set is enriched for biological processes relevant to

109 facial development and perform association mapping to highlight a list of potential causal

110 genes. In order to visualize and quantify the magnitude of marker effects on multivariate facial

111 shape (as opposed to univariate PC scores), for each QTL peak, we fit an additional mixed model

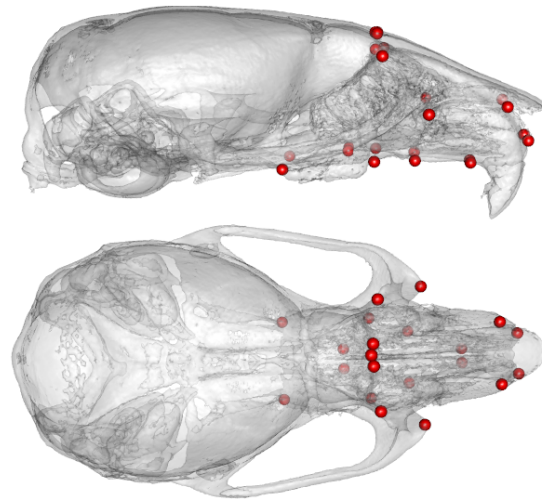112 that accommodates high-dimensional dependent observations [50].

113
114 **Fig 1. Landmark map.**

115 **Results and Discussion**

116 **QTL and Shape Variable Heritability**

117 We used a mixed effects regression model to quantify GP associations between 56,885

118 genetic markers and each of the 20 shape PCs explaining >1% of the symmetric component of

119 facial shape variation **(S1 Fig)**. Evidence for a QTL was evaluated by comparing logs odds (LOD)

120 scores (likelihood ratios comparing the magnitude of marker model residuals to the residuals of

121 a null model that excludes the marker effect) [51] at each marker to a distribution of maximum

122 LOD scores obtained from quantifying marker effects over 1000 random permutations of GP

123 assignments.

124 While comparisons to prior studies are complicated by design features unique to each,

125 the design employed here appears to have conferred benefits in terms of QTL identification and

126 localization, the primary objectives of QTL analysis [41]. From the 20 genome scans, 37 QTL

6

127   surpassed our threshold for statistical significance (95% quantile of the maximum LOD score

128   distribution). Median support interval width was 3.5 Mb (mean 7.1 Mb) using a 1.5 LOD-drop

129   threshold to define support interval boundaries. Comparable prior studies identified 17-30 QTL

130   for the skull, with a lowest median QTL interval of 7.8 Mb (using a less-demanding 1.0 LOD-drop

131   threshold) [32, 33].

132   **Fig 2** plots the support intervals for these QTL (**see also S1 Table**). The QTL span 15 of 19

133   autosomes as well as the X-chromosome. On chromosomes 7, 14, 15, and 17, QTL from

134   multiple PCs have overlapping associations with the same genomic region.
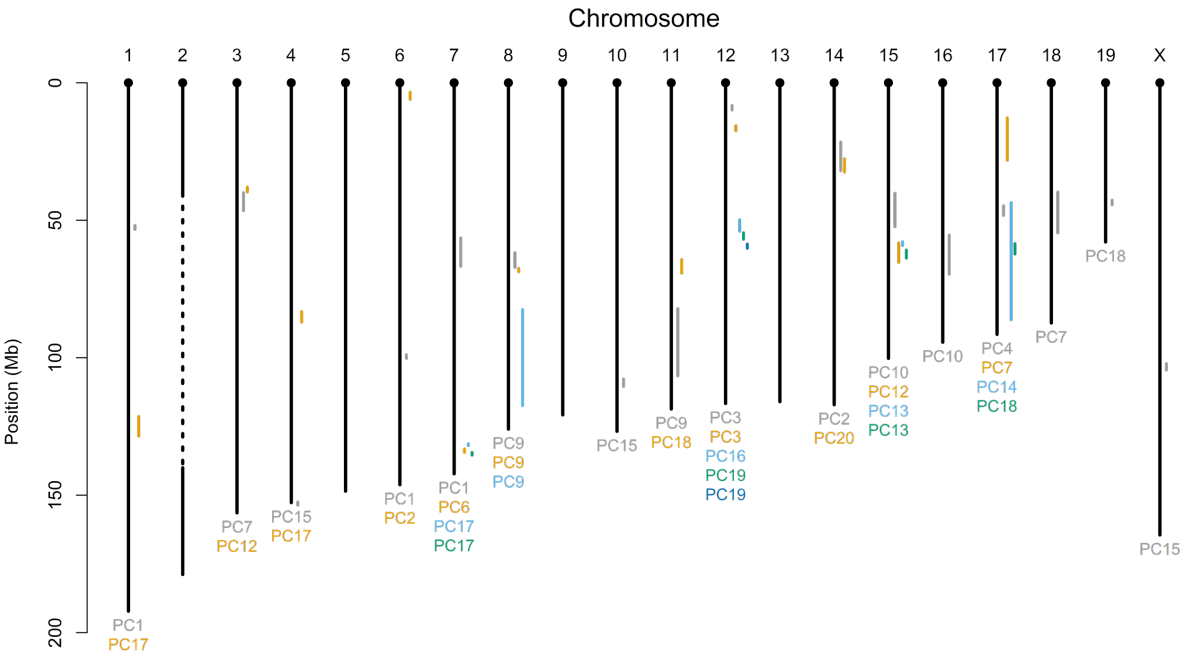

135
136
137   **Fig 2.** Mouse genome physical map with QTL support intervals. Intervals on the same
138   chromosome are color coded to match the color of the PC for which the QTL was
139   identified (listed below chromosome). The dashed line in the middle of chromosome 2
140   represents a region for which genetic effects were not evaluated due to the potential
141   effects of transmission distortion on QTL identification (see Materials & Methods for
142   further explanation).
143

7

144   For each PC, the random effect heritability estimate quantifies the proportion of

145   phenotypic variance attributable to overall genetic similarity at the founder level [49]. We

146   excluded from the genetic similarity (relatedness) calculation all markers on the same

147   chromosome as the QTL marker of interest. This leave-one-chromosome-out (LOCO) strategy

148   was chosen in order to avoid the loss of power that can arise when relatedness is computed

149   from the full complement of genotyped markers [52-54]. The LOCO approach produces a

150   unique heritability estimate for each chromosome on each PC. **Table 1** reports the mean

151   heritability for each PC, as well as the variance in these heritabilities (averaged over

152   chromosomes). For most PCs, heritability was moderately high (0.42-0.57), with a few low

153   heritability outliers. These values are very similar to those Pallares and colleagues estimated for

154   skull shape PCs in an outbred mouse sample [32], and lie mostly in the middle of the heritability

155   range for human facial shape (~30-70%) [36, 55].

156   **Table 1. Heritabilities by PC.**

	Mean h^2	Variance
PC1	0.5407	0.00012
PC2	0.4389	0.00013
PC3	0.5418	0.00022
PC4	0.3532	0.00022
PC5	0.4627	0.00012
PC6	0.5705	0.00015
PC7	0.4785	0.00014
PC8	0.4604	0.00015
PC9	0.5411	0.00032
PC10	0.5420	0.00017
PC11	0.2439	0.00009
PC12	0.4226	0.00014
PC13	0.5309	0.00013
PC14	0.4364	0.00020
PC15	0.4849	0.00005
PC16	0.4456	0.00010
PC17	0.4658	0.00020
PC18	0.4726	0.00019
PC19	0.4533	0.00006
PC20	0.5040	0.00022

157
158   Mean and variance of heritability for PC 1-20 shape traits. The full set of heritability
159   estimates is provided in **S2 Table**.
160
161   Based on signal-to-noise evaluation of shape PC eigenvalue decay [56], we limited

162 further analysis to the first five PCs (effectively four PCs, as no marker exceeded the

163 permutation significance threshold for the PC 5 shape axis). Each plot in **Fig 3** depicts the LOD

164 score profile (lower panel) and CC founder haplotype coefficients (upper panel) for a

165 chromosome harboring one or more QTL for a PC 1-4 shape variable. Shaded rectangular

166 regions delimit the 1.5-LOD drop support interval boundaries for the QTL. Founder coefficients

167 were estimated using best linear unbiased predictors [57, 58]. This helps to highlight QTL

168 regions by imposing a degree of shrinkage on the coefficients chromosome-wide [48].
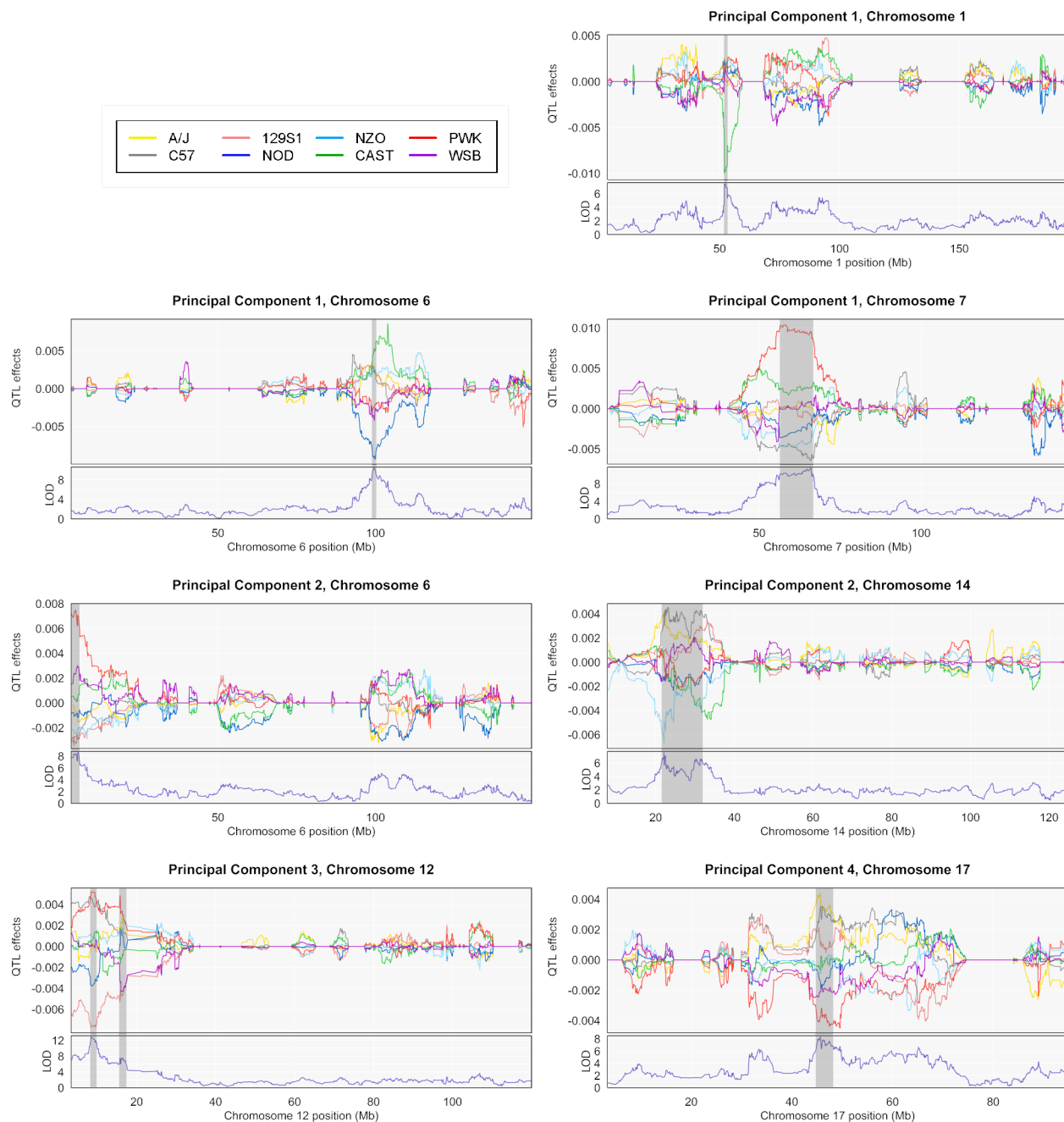
169

Fig 3. BLUP effects and LOD panels for all QTL, PCs 1-4. QTL effect colors correspond to CC founders.

We also mapped GP associations for vectors capturing covariation between shape and

two measures of size: centroid size (CS) and body mass. Shape change associated CS and body

mass variation were closely correlated with the primary axis of shape variation in our sample

176   ($r_{PC1\text{-}CS}$: 0.985, $r_{PC1\text{-}Mass}$: 0.875, $r_{CS\text{-}Mass}$: 0.927). These correlations carry forward to the QTL

177   profiles, as well. We identify two QTL each for CS and body mass allometry, one of which, on

178   chromosome 6, is common to the two allometry vectors. Together, the three QTL—on

179   chromosomes 1, 6, and 7—completely overlap with the PC 1 shape QTL (**Fig 4**).
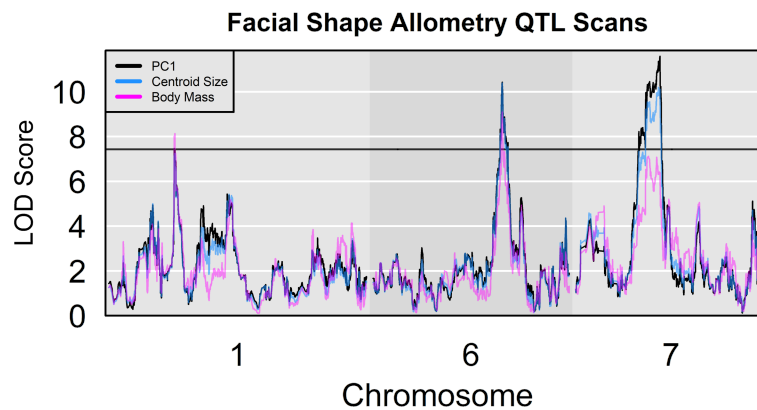

180
181   **Fig 4.** LOD plots for chromosomes containing allometry (CS and body mass) and PC 1
182   QTL. The permutation significance thresholds for all three phenotypic variables are
183   extremely similar. Only one is plotted.
184
185   The allometry results suggest a developmental model in which the determinants of

186   different size measures have partially correlated effects on cranial shape [59]. The near

187   coincidence of shape PC 1 with our explicitly allometric variables has been observed in many

188   geometric and classical morphometric investigations, and there is a long history of treating PC 1

189   as an allometry variable in morphometric analysis [59-64]. With this in mind, though primarily

190   for economy, we regard PC 1 QTL as allometry QTL in the remainder of this manuscript.
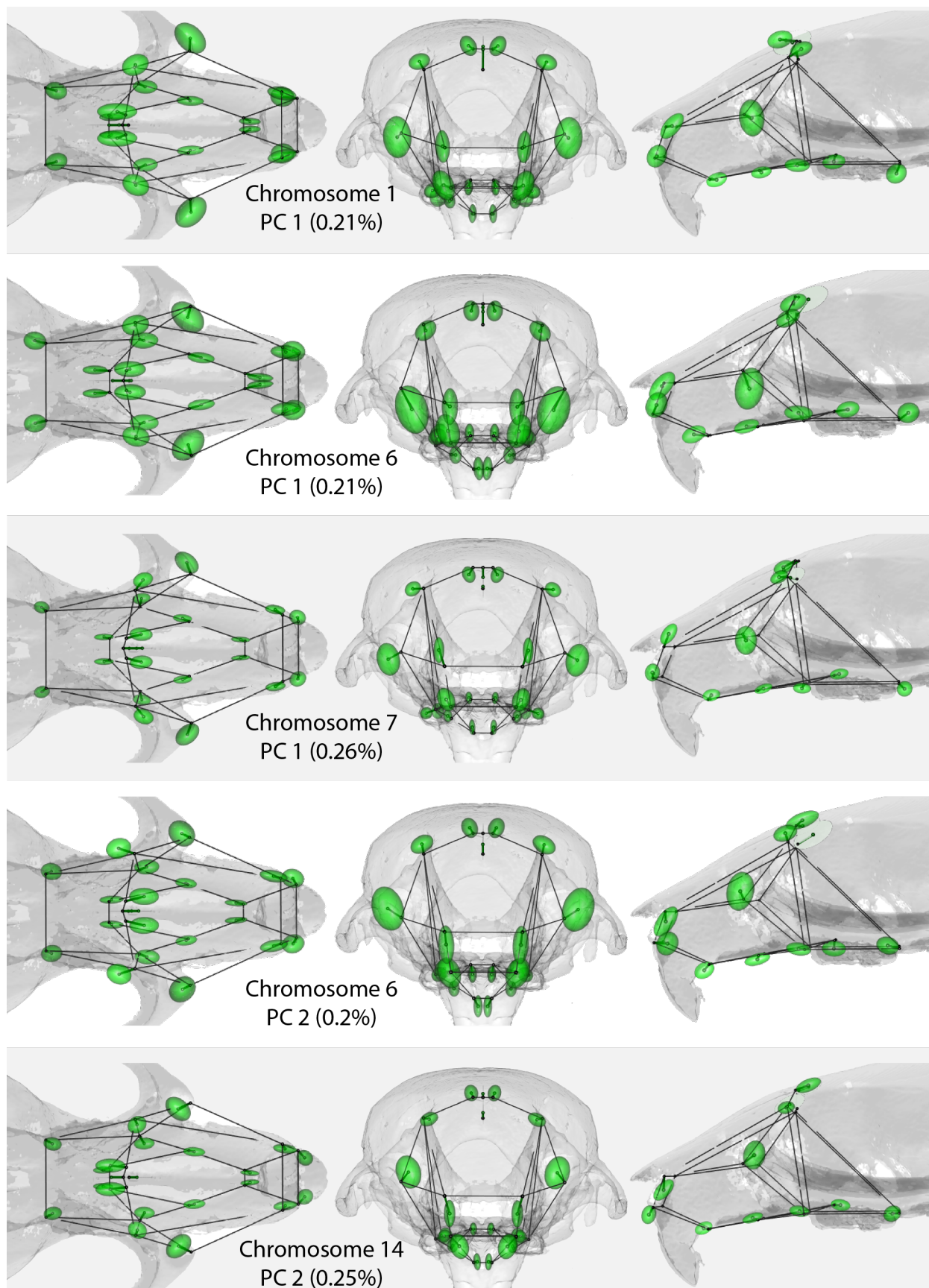
191   The mouse subspecies that comprise the CC are estimated to have diverged several

192   hundred thousand years ago [65]. In many DO studies, subspecific divergence in one or more

193   wild-derived CC lines figures prominently in the founder genetic effects contrasts that underlie

194   QTL (e.g., [66-69]). Here, the same pattern is evident for most of the PC 1-4 QTL. In six of the

195   eight QTL (or seven of nine, if the two peaks of the PC 2, chromosome 14 QTL are considered

11

196   distinct), the coefficient for a non-*domesticus* wild-derived strain (CAST or PWK) sits at one

197   extreme of the founder coefficient distribution. Only at the upstream LOD peak of the PC 2,

198   chromosome 14 QTL is the founder coefficient contrast clearly between *M.m. domesticus*

199   inbred lines. The prevalence of QTL substantially driven by wild-derived alleles highlights the

200   value of subspecific genetic diversity in the DO population.

201   The broad region of high LOD scores for PC 1 on chromosome 7 merits individual

202   attention. This QTL support interval essentially delimits the mouse homolog boundaries of the

203   human Prader-Willi/Angelman syndromes domain [70]. The founder coefficients point to a

204   strong subspecies signal, with PWK (*M.m. musculus*) highly differentiated from wild-derived

205   WSB and the inbred *M.m. domesticus* lines, and CAST (*M.m. castaneus*) intermediate. Though

206   the QTL interval contains fewer than 40 genes, nine are known to be imprinted [70-74]. Several

207   more have mixed evidence for imprinting [73], and Prader-Willi and Angelman are parent-of-

208   origin dependent neurological disorders [75]. In addition, more than a dozen genes in the

209   interval are expressed in the developing face [40, 76-81]. Our mapping strategy is not

210   specifically designed to quantify imprinted gene QTL [82-84]. However, closer dissection of this

211   interval's contribution to facial shape variation, accounting for allelic parent of origin effects,

212   may be warranted in the future. The characteristic facial phenotype for Prader-Willi includes a

213   relatively long skull with a narrow upper face [85]. In this regard, the shape effects associated

214   with the peak marker in this interval, just downstream of the primary Prader-Willi genes, are

215   suggestive, as they contrast a shorter, wider face with a longer, narrower one (see **Figs 5 and 6**,

216   below).

217   **Marker Effects on Shape**

12

218   At the LOD peak marker of each PC 1-4 QTL, we collapsed the 8-state founder

219   probabilities to 2-state SNP probabilities in order to estimate the shape effect of allelic

220   substitution at that marker. To estimate effects on total shape (instead of univariate shape

221   PCs), we employed a Bayesian mixed effects model for highly multivariate dependent

222   observations [50, 86]. The results are plotted in **Fig 5**. In each figure, QTL effects are magnified

223   by the scaling factor required to cause the QTL to account for 10% of phenotypic variance.

224   These effects are shown as displacement vectors emanating from the mean configuration

225   wireframe. The magnification ensures that even when the effect at a landmark is small, its

226   direction and relative size (in comparison to effects at other landmarks) is apparent. We further

227   exploited the Bayesian posterior to plot 80% confidence ellipsoids for the magnified

228   displacements. The actual proportion of variance explained by the SNP, without magnification,

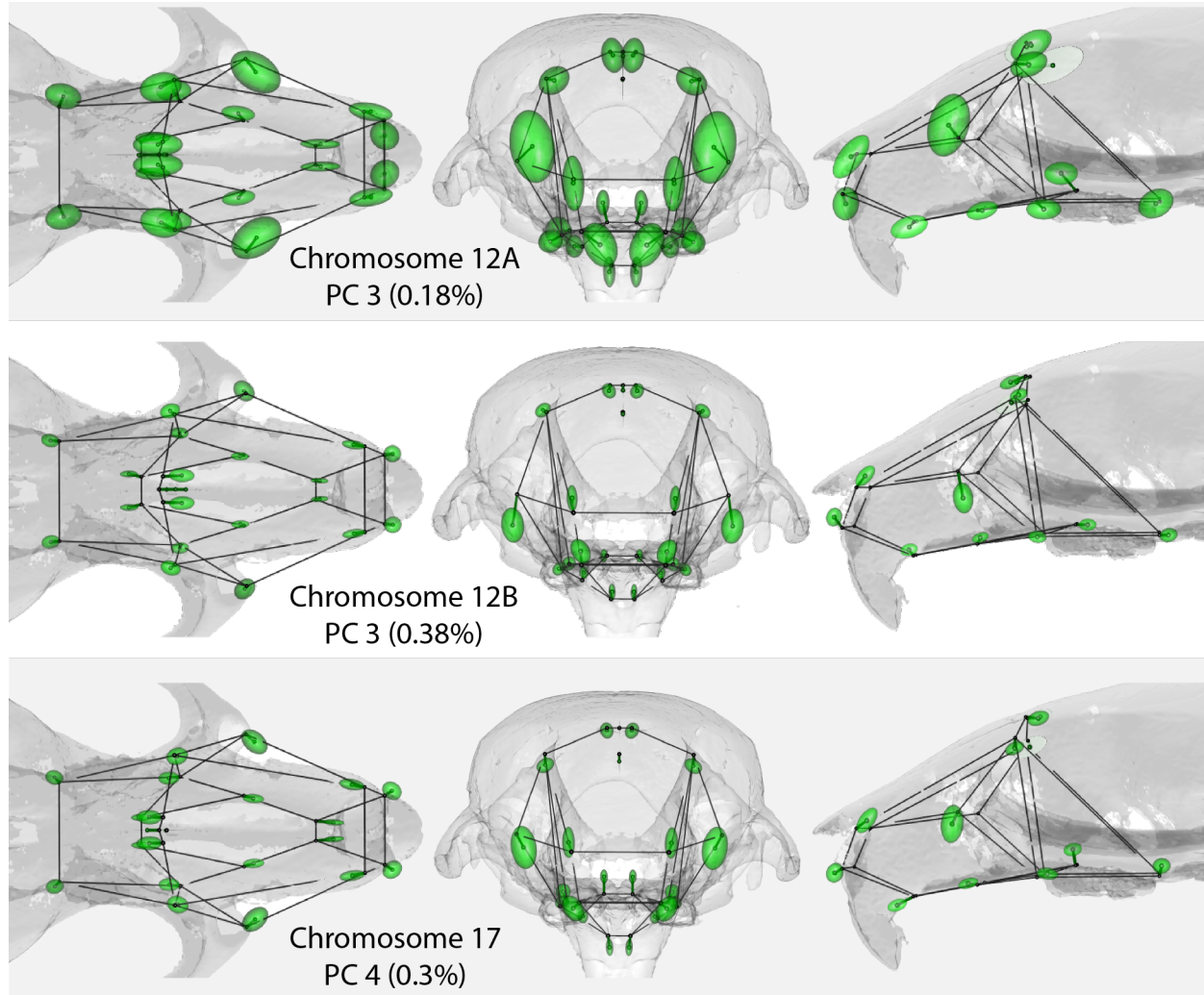229   is noted in the figure (and included in **Table 3**).

Chromosome 1
PC 1 (0.21%)

Chromosome 6
PC 1 (0.21%)

Chromosome 7
PC 1 (0.26%)

Chromosome 6
PC 2 (0.2%)

Chromosome 14
PC 2 (0.25%)

230

Chromosome 12A
PC 3 (0.18%)

Chromosome 12B
PC 3 (0.38%)

Chromosome 17
PC 4 (0.3%)

231

Fig 5. Superior (left), anterior (middle), and lateral (right) views of the (magnified) effect of allele substitution at the genome scan peak marker. Displacement vectors from wireframe to center of ellipsoids depict the mean effect. Ellipsoids enclose the approximate 80% posterior confidence boundaries.

Biological Process Enrichment

We used the human annotations in the online Molecular Signatures Database [87] to query biological processes relevant to craniofacial variation are overrepresented in the PC 1-4 QTL intervals. Collectively, the intervals contain 243 named, protein coding genes (**S1 File**), 232 of which are annotated in the Entrez Gene library utilized by the Molecular Signatures Database. **Table 2** provides GO biological process enrichment highlights for these intervals,

15

243   including FDR *q*-values adjusted for multiple testing (see **S2 File** for the top 100 *q*-value

244   processes). Growth, morphogenesis, and skeletal system development are prominent biological

245   process annotations for the facial shape QTL. The enrichment results suggest that no enriched

246   biological process is uniquely associated with shape variation on a single PC. Rather, with the

247   exception of bone development, each process in **Table 2** includes annotations to each PC.

248   **Table 2. Gene ontology enrichment for selected biological processes.**

| Biological process	FDR *q*-value	GO annotated genes
Animal organ morphogenesis	1.42 e-3	**PC1:** *Aldh1a3, Chsy1, Nab1, Stat1, Trpm1.* **PC2:** *Col1a2, Dlg5, Gngt1, Hesx1, Tnnc1, Wnt5a, Zmiz1* . **PC3:** *Gdf7, Matn3, Osr1, Sdc1.* **PC4:** *Ccdc66, Mdfi, Ptk7, Runx2, Srf, Vegfa* .
Growth	2.25 e-3	**PC1:** *Apba2, Mstn, Ndn, Nsmce3, Ube3a* . **PC2:** *Bap1, Colq, Il17rb, Mustn1, Sema3g, Tkt, Wnt5a, Zmiz1.* **PC3:** *Gdf7, Matn3, Osr1* . **PC4:** *Dnph1, Mymx, Ptk7, Srf, Taf8, Vegfa, Hsp90ab1.*
Skeletal system development	1.29 e-2	**PC1:** *Chsy1, Nab1, Foxp1, Lrrk1.* **PC2:** *Col1a2, Mustn1, Wnt5a.* **PC3:** *Matn3, Osr1, Runx2.* **PC4:** *Mdfi, Srf.*
Sensory organ development	1.62 e-2	**PC1:** *Aldh1a3, Gabra5, Gabrb3, Trpm1.* **PC2:** *Ccdc66, Gngt1, Hesx1, Wnt5a.* **PC3:** *Osr1.* **PC4:** *Prph2, Ptk7, Srf, Vegfa.*
Cartilage development	2.4 e-2	**PC1:** *Chsy1.* **PC2:** *Mustn1, Wnt5a* . **PC3:** *Matn3, Osr1.* **PC4:** *Runx2, Srf.*
Bone development	2.54 e-2	**PC1:** *Chsy1, Nab1, Lrrk1, Foxp1.* **PC3:** *Matn3.* **PC4:** *Runx2, Srf* .

249

250   To consider annotations specific to allometric variation, we queried biological process

251   enrichment for PC 1 QTL alone (**S3 File**). Collectively, the three allometry QTL intervals were

252   significantly enriched for genes implicated in bone development (FDR *q* = 0.025). Each of the

253   intervals included at least one such gene: *Nab1* (chromosome 1) [88], *Foxp1* (chromosome 6)

254   [89, 90], and *Lrrk1* and *Chsy1* (chromosome 7) [91-93]. The chromosome 1 interval also includes

255   Myostatin (*Mstn, Gdf8*), a negative regulator of muscle growth. Inactivation of *Mstn* has been

256   shown to greatly increase facial muscle mass, with corresponding size decreases and shape

257   changes throughout the bony face and vault [94, 95].

258   **Association Mapping**

259   Finally, to develop a finer-grained impression of potential causal loci, we performed SNP

260   association mapping within each QTL interval. We imputed a dense map of SNP probabilities to

261   the sample by inferring their bi-allelic (major/minor) probabilities based on (a) founder

262   probabilities at flanking, genotyped markers and (b) major/minor strain distribution patterns in

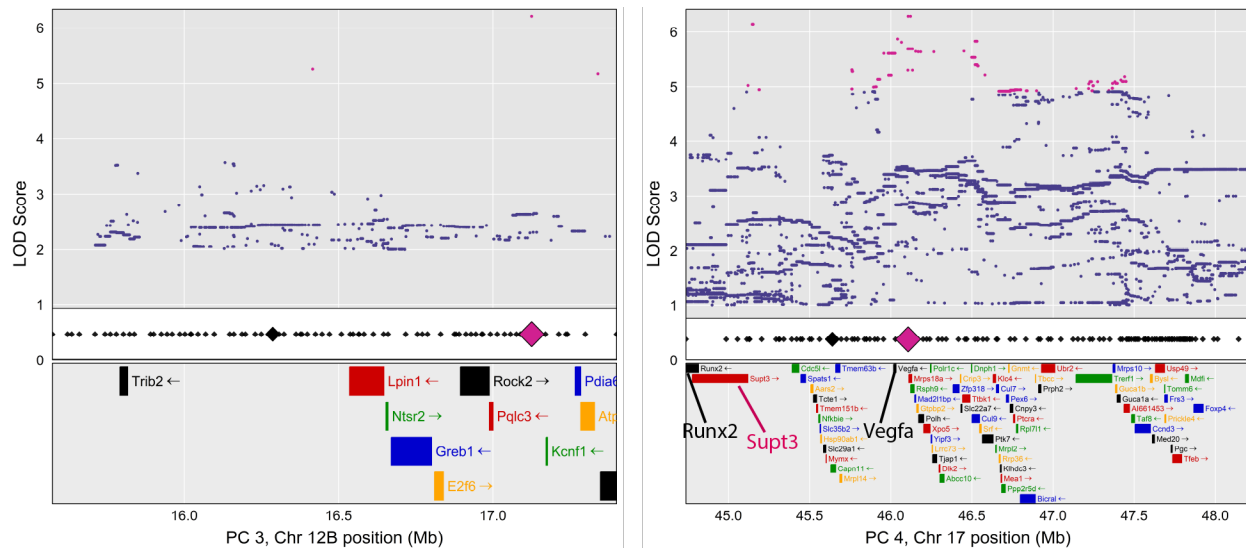263   the CC founder variants **(Fig 6)**.
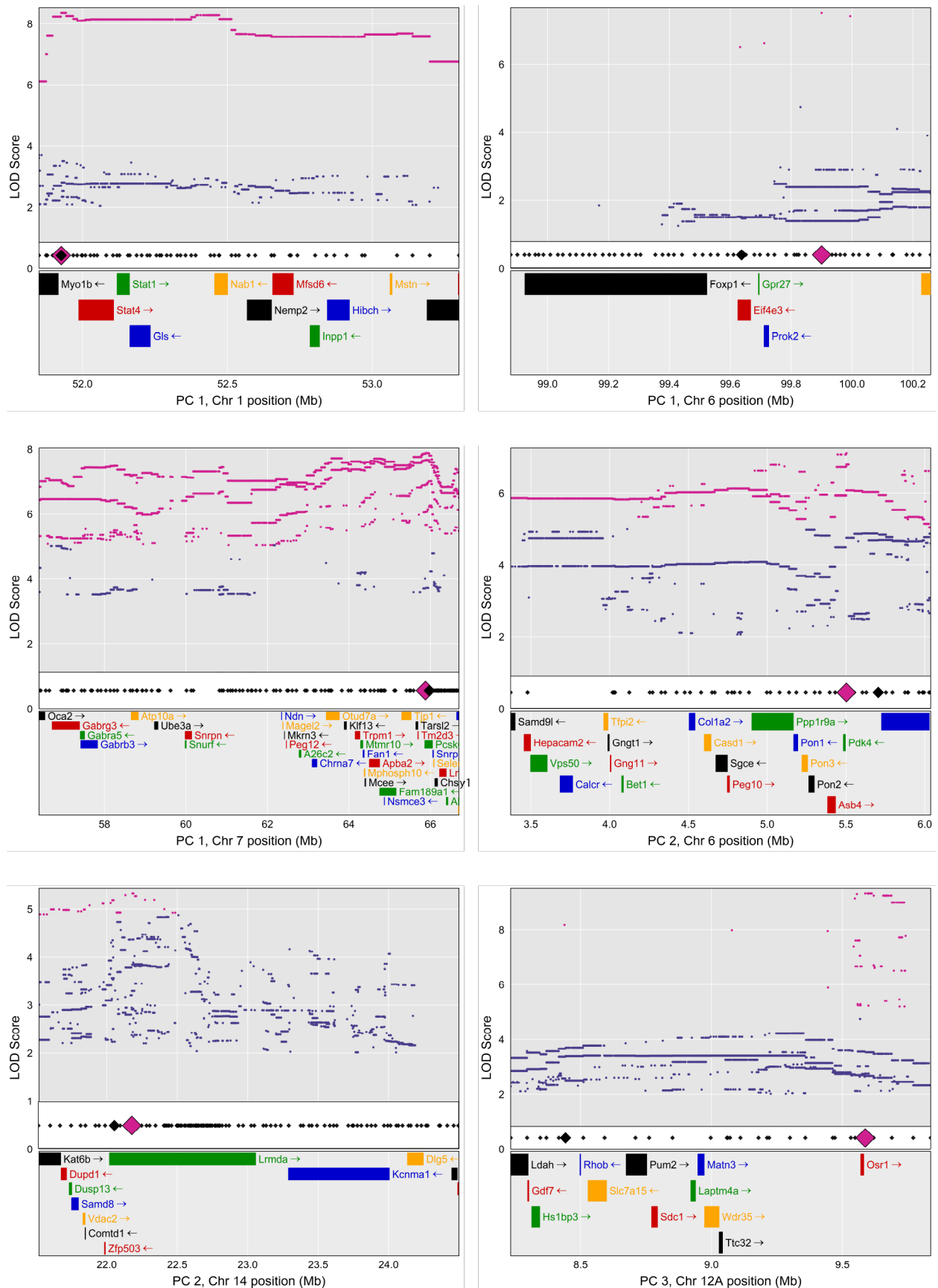
Fig 6. Association mapping results for PC 1-4 QTL intervals. Top panels: LOD scores for all CC SNP variants in the interval. Magenta points are locations where inferred bi-allelic SNP probabilities (based on strain distribution patterns in the CC) exceed the 95% LOD threshold. To control file size, low LOD scores points have been omitted from most plots. Middle panel: location of genotyped markers in the DO (small black diamonds), highlighting LOD peak locations for the founder genome scan (large black diamond) and SNP association scan (large magenta diamond). Bottom panel: named, protein coding genes for intervals. For legibility, we show the portion of the PC 2, Chromosome 14 map that contains both peak LOD scores and all SNPs exceeding the LOD threshold. For all plots, the complete gene list is provided in **S1 File**.

We then queried whether any genes within 0.25 Mb of the SNP or genome scan LOD

peaks are known to be associated with craniofacial development or phenotypes **(Table 3)**. As

with human facial shape GWAS [42], LOD peaks tended to be located in non-coding regions.

While the focal genes we identified all have known roles in skeletal or craniofacial

development, they also tend to be developmentally ubiquitous. *Stat1* (PC1, chr. 1) is implicated

in bone development and remodeling throughout life [96-98]. Overexpression of *Foxp1* (PC1,

chr. 6) can attenuate osteoblast differentiation, chondrocyte hypertrophy, osteoclastogenesis,

and bone resorption, while *Foxp1* deficiency can accelerate ossification [89, 90]. In humans,

some *Foxp1* mutations produce a facial phenotype that includes broad forehead and short nose

19

286   [99]. Chondrogenesis is generally disrupted in *Chsy1* null mouse mutants (PC1, chr. 7), and in

287   humans, *Chsy1* mutations can manifest in micrognathia and short stature [92, 100]. *Kat6b* (PC2,

288   Chr. 14) activates the transcription factor *Runx2*, which is often referred to as a master

289   regulator of bone formation [101-103]. For the PC3 QTL at 8.23 – 9.84 Mb on chromosome 12,

290   the founder and SNP LOD peaks reside at opposite ends of the QTL interval, but each is very

291   close to an important craniofacial development gene: *Gdf7* (*Bmp12*) contributes to patterning

292   of the jaw joint and is expressed in the developing incisor pulp and periodontium [104-106];

293   *Osr1* is broadly expressed in the embryonic and developing skull, with overexpression resulting

294   in intramembranous ossification deficiencies, increased chondrocyte differentiation, and

295   incomplete suture closure, while under-expression may contribute to cleft palate phenotype

296   [107-109]. *Osr1* has also previously been identified as a candidate in human facial shape GWAS

297   [23]. Finally, the SNP LOD peak for PC4, chromosome 17 implicates *Vegfa*, which is critical to

298   endochondral and intramembranous ossification through its role in angiogenesis [110]. A

299   distinct SNP LOD peak of nearly equal magnitude is located approximately 1 Mb upstream (at

300   rs47194347), very close to *Supt3* (human ortholog *Supt3h*) and *Runx2*. In addition to the central

301   role *Runx2* has in bone formation and development [102], both genes are human facial shape

302   GWAS candidates [15, 22].

303   **Table 3. Candidate genes.**

PC	Chr	Founder Peak (Mb)	Founder ID	Founder type	SNP Peak (Mb)	SNP ID	SNP_type	SNP % Var	Candidates
PC1	1	51.926616	rs48415864	intergenic	51.926623	rs254750887	intergenic	0.21	*STAT1*
PC1	6	99.637221	rs226005706	intron	99.900271	rs31234872	intergenic	0.21	*FOXP1*
PC1	7	65.970847	rs33905059	intron	65.876674	rs32405988	intron	0.26	*CHSY1*
PC2	6	5.704731	rs49620919	intergenic	5.502445	rs32485785	intergenic	0.2	NA
PC2	14	22.058402	rs30739483	intron	22.182166	rs30740474	intron	0.25	*KAT6B*
PC3	12	8.44203	rs48833407	intergenic	9.587123	rs29212735	intergenic	0.18	*OSR1, GDF7*
PC3	12	16.286802	rs49949506	intergenic	17.125642	SV 17121898: 17129386	structural (deletion)	0.38	NA
PC4	17	45.639772	rs107675960	intron	46.106749	rs108721614	upstream gene variant	0.3	*VEGFA [RUNX2, SUPT3]*

304

305 Candidate genes located within 0.25 Mb of founder or SNP QTL peaks. SNP % Var gives
306 the percentage of variation explained by substitution of an additional reference allele at
307 the founder (genome scan) peak.
308

309 While GP maps for traits influenced by many genes may be quite intricate and layered,

310 additive effect QTL analyses remain an indispensable means to identify loci that contribute to

311 phenotypic variation. Our investigation advances understanding of the genetics of facial

312 skeletal diversity in several ways. The 37 QTL identified herein substantially expand the small

313 but growing facial shape QTL library. Compared to similar prior studies, the number of QTL is

314 relatively large and their confidence intervals relatively narrow. These results affirm the value

315 of larger samples, sophisticated animal models like the outcrossed population utilized here, and

316 high-resolution genotyping for identification and localization of QTL. Synthesizing our results

317 with prior insights from developmental biology and medical genetics provides a richer picture

318 of the sources of facial skeletal diversity. We found a relative abundance of skeletal and

319 craniofacial development genes in QTL intervals for the largest shape PCs. Moreover, these

320 genes tend to be located very close to QTL peaks. Thus, our results suggest that genes essential

321 to building a face are often also the genes that cause faces to vary. Finally, QTL effect sizes were

322 small. In summary, our results are consistent with a model of facial diversity that is influenced

323 by key genes in skeletal and facial development and, simultaneously, highly polygenic.

21

Materials and methods

Diversity Outbred mouse population

The DO (Jackson Laboratory, www.jax.org) are derived from the eight inbred founder

lines that contribute to the CC [43, 44], which include three mouse subspecies, and both wild-

derived and laboratory strains [46]. Continued random outcrossing of the DO has produced a

population with relatively high genetic diversity (~45 million SNPs segregating in the CC

founding populations [43]) and increasingly fine mapping resolution in advancing generations.

In combination, these features increase the potential to identify multiple QTL for

complex traits [31]. On average, the genomes of the eight CC founders should be equally

represented in the DNA of any DO animal. Sequenced genomes for the CC make it possible to

characterize and interpret genetic variants in the DO according to 8-state founder identity and

as bi-allelic (major/minor allele) SNP variation. In addition, statistical packages designed for

analysis of the DO offer features to impute variants at each typed SNP in the CC founders, using

the coarser DO marker map as a scaffold to infer a high-density SNP map.

Computing

All analysis was conducted in R [111]. Customized data processing and statistical analysis

functions for mapping experiments in DO samples were originally published in the DOQTL

package [49]. These routines are now incorporated into the qlt2 package [48], with additional

processing and genotype diagnostic tools provided at https://kbroman.org/qtl2/.

Images, landmark data

Our DO sample consists of *n*=1147 male and female adult mice (after exclusion of some

records; see *Genotypes*, below) from seven DO generations (**Table 4**). We obtained μCT images

346   of the mouse skulls in the 3D Morphometrics Centre at the University of Calgary on a Scanco

347   vivaCT40 scanner (Scanco Medical, Brüttisellen, Switzerland) at 0.035 mm voxel dimensions at

348   55kV and 72-145 µA. On each skull, one of us (WL) collected 54 3D landmark coordinates from

349   minimum threshold-defined bone surface with ANALYZE 3D (www.mayo.edu/bir/). Here, we

350   analyzed the 22-landmark subset of the full configuration—a 66 coordinate dimension vector—

351   that captures the shape of the face (**Fig 1**).

352   **Table 4. DO sample composition.**

	DO generation						
	9	**10**	**15**	**19**	**21**	**23**	**27**
Female	91	221	80	55	80	97	75
Male	0	144	0	58	77	99	70
MUGA Array	Mega	Mega	Mega	Giga	Giga	Giga	Giga

353
354   Overview of the DO sample by generation, sex, and genotyping array.
355
356   **Ethics Statement**

357   No animals were sacrificed for this study. Specimens were raised in several labs for

358   unrelated experiments under approval and conduced in accordance with the guidelines set

359   forth by the Institutional Animal Care and Use Committee in accordance with protocols #11-299

360   (University of North Carolina Chapel Hill), #99066 and #15026 (Jackson Labs), and #08-0150-3

361   (Scripps Research Institute). Receipt of animal carcasses and micro-CT (µCT) imaging of mouse

362   skulls were undertaken in accordance with approved IACUC protocol #AC18-0026 at the

363   University of Calgary.

364   **Shape data**

365   Landmark configurations were symmetrically superimposed by Generalized Procrustes

366   Analysis (GPA) [112] using the Morpho package [113]. GPA is a multi-step procedure that

367   removes location and centroid size differences between configurations, then (iteratively)

23

368 rotates each configuration to minimize its squared distance from the sample mean. We chose a

369 superimposition that decomposes shape variation into its symmetric and asymmetric

370 components [114, 115], and stored the symmetric configurations for analysis. Working with

371 symmetric, superimposed data reduced morphological degrees of freedom from 66 landmark

372 coordinate dimensions to 30 shape dimensions [115].

373 **Genotypes**

374 For all animals, DNA was extracted from ear or tail clippings. Genotyping was performed

375 by the Geneseek operations of Neogen Corp. (Lincoln, NE). Mice from generations 9, 10, and 15

376 were genotyped using the MegaMUGA genotyping array (77,808 markers); mice from

377 generations 19, 21, 23, and 27 were genotyped using the larger GigaMUGA array (143,259

378 markers) [116]. The two arrays share 58,907 markers in common. We restricted the genotype

379 data to these shared SNPs [116].

380 In addition, we excluded 2,022 markers from the center of chromosome 2 (40 - 140

381 Mb). WSB alleles are highly overrepresented in this genomic region in earlier DO generations.

382 This overrepresentation has been attributed to female meiotic drive favoring WSB at the *R2d2*

383 locus [117]. Between DO generations 12 and 21, Jackson Labs systematically purged the meiotic

384 drive locus and linked effects from the DO [45]. Our samples closely track this history, with WSB

385 allele frequencies in the middle of chromosome 2 exceeding 60% in generation 9 and falling to

386 0% by generation 23 (**S2 Fig**). If unaddressed, this directional shift in allele frequencies can

387 confound statistical analysis of genotype-phenotype associations [118] with potentially false

388 positive associations between WSB chromosome 2 haplotypes and directional changes in

389 phenotype over DO generations. After removing this genomic region from consideration, the

390   final SNP dataset consists of 56,885 markers common to the MegaMUGA and GigaMUGA

391   arrays, with a mean spacing of 48 kb.

392   The qtl2 package estimates genotype probabilities, including imputation of sporadically

393   missing genotypes, with a multipoint Hidden Markov Model (HMM) on the observed marker

394   genotypes. From these initial genotype probabilities, we derived three probabilistic

395   representations of genetic state for each observation at each marker: (1) for genome scans,

396   founder probabilities, a vector encoding the probability of genetic contribution from each of

397   the eight CC founders to the diplotype state; (2) for association mapping, SNP probabilities,

398   collapsing the eight founder probabilities to a two-state, major/minor allele strain distribution;

399   and (3) for mapping multivariate shape effects, additive SNP dosage, twice the estimated major

400   SNP probability (maximum additive SNP dosage = 2).

401   We identified problematic genetic samples using the DO genotype diagnostics tools

402   available at https://kbroman.org/qtl2/ [119]. A total of 11 observations were excluded due to

403   excessive missing marker data, which we defined as no marker information at >7.5% of

404   markers. Three probable duplicate sets of genetic data (>99% of markers identical) were

405   identified. Because the correct genotype-phenotype matches could not be established by other

406   evidence, all six animals were removed from the sample. Finally, we excluded seven female

407   samples with low X chromosome array intensity values. These samples are potentially XO [45],

408   which can affect facial form and body size [120, 121]. The exclusions described above resulted

409   in a final, retained sample of n = 1147 animals.

410   **Genome scan and association mapping**

411   We mapped QTL for facial shape and facial shape allometry. To identify QTL, we

412   implemented the linear mixed effects regression model in qtl2. The qtl2 genome scan is

413   designed to estimate marker effects on one or more univariate observations, but not

414   covariance among those dimensions. We therefore decomposed the superimposed coordinates

415   into PCs, treating the specimen scores on each PC as measured traits. For allometry, we treated

416   common allometric component scores [61] as measured traits. Prior to deriving PCs and

417   allometry vectors, we centered each observation on its generation mean in order to focus on

418   shared, within-generation covariance patterns [122, p. 295].

419   At each marker, we fit a mixed model with fixed effect coefficients for sex, age-at-

420   sacrifice, and the additive effect of each CC founder haplotype, a random effect of kinship, and

421   an error term [49]. Evidence for a QTL was evaluated based on marker LOD scores, likelihood

422   ratios comparing the residuals of the marker model to a null model excluding the marker's

423   effect [51]. We consider the evidence for a marker-phenotype association to be statistically

424   significant where the LOD score exceeds the 95% quantile of genome-wide maximum LOD

425   scores computed from 1000 random permutations of genotype-phenotype associations [123].

426   We use a 1.5 LOD-drop rule to define the boundaries of QTL support intervals [124], and allow

427   for multiple QTL peaks on a single chromosome.

428   The random effect of kinship depends upon pairwise proportions of shared alleles

429   among observations, encoded in a kinship matrix. Loss of power to detect QTL can arise when

430   the marker of interest and linked genes are included in the kinship matrix of the null model. To

431   avoid this problem, we compute kinship matrices using a leave-one-chromosome-out (LOCO)

432   approach [52-54].

433   Genome scans, QTL support intervals, and proportions of shape variation attributable to

434   founder-level kinship (heritability) were estimated for all PCs explaining more than 1% of

435   symmetric shape variation. However, we limit more in-depth analysis to the five PCs with

436   reasonably large signal-to-noise ratios (**S2 Fig**). This was assessed using the modified "noise

437   floor" detection strategy developed by Marroig and colleagues in [56].

438   In addition, within the PC 1-5 QTL intervals, we used a form of merge analysis to

439   perform genome-wide association mapping [49, 125, 126]. For each CC founder variant located

440   between a flanking pair of genotyped markers, the vector of founder allele probabilities is

441   assumed to be the average of the founder probabilities at those flanking markers. The bi-allelic

442   SNP probabilities were computed from these founder probabilities and the major/minor allele

443   strain distribution pattern in the CC. Analysis was again via mixed effects regression model, with

444   the imputed SNP data as genotype predictors.

445   **Enrichment analysis and candidate genes**

446   Modern GWAS and QTL studies often attempt to contextualize QTL and candidate gene

447   results post hoc via GO enrichment analysis. Given a list of genes near statistically significant

448   markers, a GO analysis calculates the probability that a random set of genes of the same size

449   would contain as many genes under a common annotation term, typically after a family-wise

450   error rate or FDR adjustment for multiple testing. The outcome of enrichment analysis is a list

451   of GO terms (or in the absence of any enrichment, no list), which provides a means to consider

452   whether certain biological processes, cellular components, or molecular functions are over-

453   represented in the list of genes [127].

27

454   For protein coding genes in the PC 1-5 QTL support intervals and for allometry QTL, we

455   used the Molecular Signatures Database [87] online tool and Entrez Gene library [128] to

456   identify biological process GO term enrichment [129]. The database application implements a

457   hypergeometric test of statistical significance, quantifying the probability of sampling, without

458   replacement, as many (k) or more genes annotated to a GO term, given the total number of

459   genes annotated to that term (K) and the number of genes in the QTL and Entrez gene sets (n

460   and N, respectively). For each ontology term, after adjustment for multiple testing, we required

461   a FDR q-value < 0.05 to conclude that there was substantial evidence for GO biological process

462   enrichment. We also inspected the association mapping results in the +/- 0.25 Mb region

463   centered at each LOD peak for genes with convincing evidence of a role in skeletal, craniofacial,

464   or dental development or disease. For most QTL, LOD peaks for the genome scan and

465   association mapping results are virtually coincident. Where they differ substantially, we

466   examine the region around both peaks.

467   **Marker effects on shape**

468   We considered a significant association between a marker and facial shape along a PC

469   axis to be evidence of some effect on the multivariate (undecomposed) shape coordinate data.

470   In order to obtain an estimate of the full shape effect, we fit an additional mixed model for the

471   maximum LOD score marker. Fitting a mixed model for highly multivariate data presents a

472   significant computational challenge because the number of parameters that must be estimated

473   for the random effects covariance matrix scales quadratically with the number of traits (here,

474   465 parameters for 30 free variables). To address this challenge, we estimated mixed model

475   covariance matrices using a Bayesian sparse factorization approach [50, 86, 130]. After a

476   1,000,000 iteration burn-in, we generated 1,000,000 realizations from a single Markov chain,

477   thinning at a rate of 1,000 to store 1,000 posterior samples for inference. Though the time

478   needed to fit such a model makes it impractical for a genome scan on a dense array, it is a

479   useful strategy for disentangling kinship from the effect on multivariate outcomes at a small

480   number of peak markers. For these regressions, the marker effect predictor was twice the

481   major SNP probability. Thus, the multivariate mixed model we implemented estimates an

482   average effect of allele substitution, a standard quantity in quantitative genetics [131]. In

483   addition, for each regression, we estimated the proportion of shape variation explained using a

484   version of the coefficient of determination (R^2) that has been adapted for mixed model

485   parameters [132].

486   When plotting shape effects, we magnify the allele substitution coefficients by the

487   scaling factor needed to cause the QTL to explain 5% of phenotypic variance. This magnification

488   is applied both to the mean effect, in order to depict the mean displacement vector, and to the

489   posterior distribution of effects, in order to depict confidence ellipsoids. Ellipsoids were

490   estimated with the 3D ellipse function in the R package rgl [133]. While it is more typical to use

491   a 95% support boundary to evaluate effect uncertainty, with shape data, morphological

492   contrasts are best understood over the configuration as a whole [134]. The 80% ellipsoids are

493   meant to encourage this perspective.

494

495   **Acknowledgements**

29

498   and Kuo-Chen Jung for assistance with UNC mouse experiments. Charles Farber is gratefully

499   acknowledged for assistance with processing of UNC mouse carcasses. All UNC mouse

500   procedures were approved and guided by the appropriate institutional animal ethics

501   committees, including the University of North Carolina at Chapel Hill.

502

503   **REFERENCES**

504   1.   Hu D, Marcucio RS. A SHH-responsive signaling center in the forebrain regulates
505   craniofacial morphogenesis via the facial ectoderm. Development. 2009;136(1):107-16. Epub
506   2008/11/26. doi: 10.1242/dev.026583. PubMed PMID: 19036802; PubMed Central PMCID:
507   PMCPMC2685963.
508   2.   Hallgrímsson B, Jamniczky H, Young NM, Rolian C, Parsons TE, Boughner JC, et al.
509   Deciphering the palimpsest: studying the relationship between morphological integration and
510   phenotypic covariation. Evolutionary Biology. 2009;36(4):355-76.
511   3.   Hallgrimsson B, Mio W, Marcucio RS, Spritz R. Let's face it--complex traits are just not
512   that simple. PLoS Genet. 2014;10(11):e1004724. Epub 2014/11/06. doi:
513   10.1371/journal.pgen.1004724. PubMed PMID: 25375250; PubMed Central PMCID:
514   PMCPMC4222688.
515   4.   Varón-González C, Pallares LF, Debat V, Navarro N. Mouse Skull Mean Shape and Shape
516   Robustness Rely on Different Genetic Architectures and Different Loci. Front Genet. 2019;10:64.
517   Epub 2019/02/12. doi: 10.3389/fgene.2019.00064. PubMed PMID: 30809244; PubMed Central
518   PMCID: PMCPMC6379267.
519   5.   Young NM, Chong HJ, Hu D, Hallgrímsson B, Marcucio RS. Quantitative analyses link
520   modulation of sonic hedgehog signaling to continuous variation in facial growth and shape.
521   Development. 2010;137(20):3405-9. Epub 2010/09/08. doi: 10.1242/dev.052340. PubMed
522   PMID: 20826528; PubMed Central PMCID: PMCPMC2947484.
523   6.   Green RM, Fish JL, Young NM, Smith FJ, Roberts B, Dolan K, et al. Developmental
524   nonlinearity drives phenotypic robustness. Nat Commun. 2017;8(1):1970. Epub 2017/12/06.
525   doi: 10.1038/s41467-017-02037-7. PubMed PMID: 29213092; PubMed Central PMCID:
526   PMCPMC5719035.
527   7.   Mitteroecker P, Bookstein F. The Conceptual and Statistical Relationship between
528   Modularity and Morphological Integration. Systematic Biology. 2007;56(5):818-36. doi:
529   10.1080/10635150701648029.
530   8.   Szabo-Rogers HL, Smithers LE, Yakob W, Liu KJ. New directions in craniofacial
531   morphogenesis. Dev Biol. 2010;341(1):84-94. Epub 2009/11/24. doi:
532   10.1016/j.ydbio.2009.11.021. PubMed PMID: 19941846.
533   9.   Francis-West P, Crespo-Enriquez I. Vertebrate Embryo: Craniofacial Development. eLS
534   [Internet]. 2016:[1-15 pp.].

535   10.   Falconer DS, Mackay TF. Introduction to quantitative genetics. 4th ed. Essex: Pearson
536   Education Limited; 2009.

537   11.   Huang W, Mackay TF. The Genetic Architecture of Quantitative Traits Cannot Be Inferred
538   from Variance Component Analysis. PLoS Genet. 2016;12(11):e1006421. Epub 2016/11/03. doi:
539   10.1371/journal.pgen.1006421. PubMed PMID: 27812106; PubMed Central PMCID:
540   PMCPMC5094750.

541   12.   Barton NH, Keightley PD. Understanding quantitative genetic variation. Nat Rev Genet.
542   2002;3(1):11-21. doi: 10.1038/nrg700. PubMed PMID: 11823787.

543   13.   Varón-González C, Navarro N. Epistasis regulates the developmental stability of the
544   mouse craniofacial shape. Heredity (Edinb). 2019;122(5):501-12. Epub 2018/09/12. doi:
545   10.1038/s41437-018-0140-8. PubMed PMID: 30209292; PubMed Central PMCID:
546   PMCPMC6461946.

547   14.   Wolf JB, Leamy LJ, Routman EJ, Cheverud JM. Epistatic pleiotropy and the genetic
548   architecture of covariation within early and late-developing skull trait complexes in mice.
549   Genetics. 2005;171(2):683-94. Epub 2005/07/14. doi: 10.1534/genetics.104.038885. PubMed
550   PMID: 16020793; PubMed Central PMCID: PMCPMC1456798.

551   15.   Claes P, Roosenboom J, White JD, Swigut T, Sero D, Li J, et al. Genome-wide mapping of
552   global-to-local genetic effects on human facial shape. Nat Genet. 2018;50(3):414-23. Epub
553   2018/02/19. doi: 10.1038/s41588-018-0057-4. PubMed PMID: 29459680; PubMed Central
554   PMCID: PMCPMC5937280.

555   16.   Lee MK, Shaffer JR, Leslie EJ, Orlova E, Carlson JC, Feingold E, et al. Genome-wide
556   association study of facial morphology reveals novel associations with FREM1 and PARK2. PLoS
557   One. 2017;12(4):e0176566. Epub 2017/04/25. doi: 10.1371/journal.pone.0176566. PubMed
558   PMID: 28441456; PubMed Central PMCID: PMCPMC5404842.

559   17.   Liu F, van der Lijn F, Schurmann C, Zhu G, Chakravarty MM, Hysi PG, et al. A genome-
560   wide association study identifies five loci influencing facial morphology in Europeans. PLoS
561   Genet. 2012;8(9):e1002932. Epub 2012/09/13. doi: 10.1371/journal.pgen.1002932. PubMed
562   PMID: 23028347; PubMed Central PMCID: PMCPMC3441666.

563   18.   Paternoster L, Zhurov AI, Toma AM, Kemp JP, St Pourcain B, Timpson NJ, et al. Genome-
564   wide association study of three-dimensional facial morphology identifies a variant in PAX3
565   associated with nasion position. Am J Hum Genet. 2012;90(3):478-85. Epub 2012/02/16. doi:
566   10.1016/j.ajhg.2011.12.021. PubMed PMID: 22341974; PubMed Central PMCID:
567   PMCPMC3309180.

568   19.   Shaffer JR, Orlova E, Lee MK, Leslie EJ, Raffensperger ZD, Heike CL, et al. Genome-Wide
569   Association Study Reveals Multiple Loci Influencing Normal Human Facial Morphology. PLoS
570   Genet. 2016;12(8):e1006149. Epub 2016/08/25. doi: 10.1371/journal.pgen.1006149. PubMed
571   PMID: 27560520; PubMed Central PMCID: PMCPMC4999139.

572   20.   Crouch DJM, Winney B, Koppen WP, Christmas WJ, Hutnik K, Day T, et al. Genetics of the
573   human face: Identification of large-effect single gene variants. Proc Natl Acad Sci U S A.
574   2018;115(4):E676-E85. Epub 2018/01/04. doi: 10.1073/pnas.1708207114. PubMed PMID:
575   29301965; PubMed Central PMCID: PMCPMC5789906.

576   21.   Cole JB, Manyama M, Kimwaga E, Mathayo J, Larson JR, Liberton DK, et al. Genomewide
577   Association Study of African Children Identifies Association of SCHIP1 and PDE8A with Facial
578   Size and Shape. PLoS Genet. 2016;12(8):e1006174. Epub 2016/08/25. doi:

31

579   10.1371/journal.pgen.1006174. PubMed PMID: 27560698; PubMed Central PMCID:
580   PMCPMC4999243.
581   22.   Adhikari K, Fuentes-Guajardo M, Quinto-Sánchez M, Mendoza-Revilla J, Camilo Chacón-
582   Duque J, Acuña-Alonzo V, et al. A genome-wide association scan implicates DCHS2, RUNX2,
583   GLI3, PAX1 and EDAR in human facial variation. Nat Commun. 2016;7:11616. Epub 2016/05/19.
584   doi: 10.1038/ncomms11616. PubMed PMID: 27193062; PubMed Central PMCID:
585   PMCPMC4874031.
586   23.   Cha S, Lim JE, Park AY, Do JH, Lee SW, Shin C, et al. Identification of five novel genetic
587   loci related to facial morphology by genome-wide association studies. BMC Genomics.
588   2018;19(1):481. Epub 2018/06/19. doi: 10.1186/s12864-018-4865-9. PubMed PMID: 29921221;
589   PubMed Central PMCID: PMCPMC6008943.
590   24.   Richmond S, Howe LJ, Lewis S, Stergiakouli E, Zhurov A. Facial Genetics: A Brief
591   Overview. Front Genet. 2018;9:462. Epub 2018/10/16. doi: 10.3389/fgene.2018.00462.
592   PubMed PMID: 30386375; PubMed Central PMCID: PMCPMC6198798.
593   25.   Cole J, Spritz RA. The genetics of facial morphology. eLS [Internet]. 2017:[1-9 pp.].
594   26.   Cheverud JM, Routman EJ, Irschick DJ. PLEIOTROPIC EFFECTS OF INDIVIDUAL GENE LOCI
595   ON MANDIBULAR MORPHOLOGY. Evolution. 1997;51(6):2006-16. doi: 10.1111/j.1558-
596   5646.1997.tb05122.x. PubMed PMID: 28565113.
597   27.   Kenney-Hunt JP, Wang B, Norgard EA, Fawcett G, Falk D, Pletscher LS, et al. Pleiotropic
598   patterns of quantitative trait loci for 70 murine skeletal traits. Genetics. 2008;178(4):2275-88.
599   doi: 10.1534/genetics.107.084434. PubMed PMID: 18430949; PubMed Central PMCID:
600   PMCPMC2323815.
601   28.   Pallares LF, Harr B, Turner LM, Tautz D. Use of a natural hybrid zone for genomewide
602   association mapping of craniofacial traits in the house mouse. Mol Ecol. 2014;23(23):5756-70.
603   Epub 2014/11/15. doi: 10.1111/mec.12968. PubMed PMID: 25319559.
604   29.   Klingenberg CP, Leamy LJ. Quantitative genetics of geometric shape in the mouse
605   mandible. Evolution. 2001;55(11):2342-52. doi: 10.1111/j.0014-3820.2001.tb00747.x.
606   30.   Klingenberg CP, Leamy LJ, Cheverud JM. Integration and Modularity of Quantitative Trait
607   Locus Effects on Geometric Shape in the Mouse Mandible. Genetics. 2004;166(4):1909-21. doi:
608   10.1534/genetics.166.4.1909.
609   31.   Flint J, Eskin E. Genome-wide association studies in mice. Nat Rev Genet.
610   2012;13(11):807-17. Epub 2012/10/09. doi: 10.1038/nrg3335. PubMed PMID: 23044826;
611   PubMed Central PMCID: PMCPMC3625632.
612   32.   Pallares LF, Carbonetto P, Gopalakrishnan S, Parker CC, Ackert-Bicknell CL, Palmer AA, et
613   al. Mapping of Craniofacial Traits in Outbred Mice Identifies Major Developmental Genes
614   Involved in Shape Determination. PLoS Genet. 2015;11(11):e1005607. Epub 2015/11/02. doi:
615   10.1371/journal.pgen.1005607. PubMed PMID: 26523602; PubMed Central PMCID:
616   PMCPMC4629907.
617   33.   Maga AM, Navarro N, Cunningham ML, Cox TC. Quantitative trait loci affecting the 3D
618   skull shape and size in mouse and prioritization of candidate genes in-silico. Front Physiol.
619   2015;6:92. Epub 2015/03/26. doi: 10.3389/fphys.2015.00092. PubMed PMID: 25859222;
620   PubMed Central PMCID: PMCPMC4374467.
621   34.   Percival CJ, Green R, Roseman CC, Gatti DM, Morgan JL, Murray SA, et al.
622   Developmental constraint through negative pleiotropy in the zygomatic arch. Evodevo.

623   2018;9:3. Epub 2018/01/27. doi: 10.1186/s13227-018-0092-3. PubMed PMID: 29423138;
624   PubMed Central PMCID: PMCPMC5787316.
625   35.   Gudbjartsson DF, Walters GB, Thorleifsson G, Stefansson H, Halldorsson BV,
626   Zusmanovich P, et al. Many sequence variants affecting diversity of adult human height. Nat
627   Genet. 2008;40(5):609-15. Epub 2008/04/06. doi: 10.1038/ng.122. PubMed PMID: 18391951.
628   36.   Cole J, Manyama M, Larson JR, Liberton DK, Ferrara TM, Riccardi SL, et al. Human Facial
629   Shape and Size Heritability and Genetic Correlations. Genetics. 2017;205(2):967-78. Epub
630   2016/12/14. doi: 10.1534/genetics.116.193185. PubMed PMID: 27974501; PubMed Central
631   PMCID: PMCPMC5289863.
632   37.   de Los Campos G, Vazquez AI, Hsu S, Lello L. Complex-Trait Prediction in the Era of Big
633   Data. Trends Genet. 2018;34(10):746-54. Epub 2018/08/20. doi: 10.1016/j.tig.2018.07.004.
634   PubMed PMID: 30139641; PubMed Central PMCID: PMCPMC6150788.
635   38.   Wilderman A, VanOudenhove J, Kron J, Noonan JP, Cotney J. High-Resolution
636   Epigenomic Atlas of Human Embryonic Craniofacial Development. Cell Rep. 2018;23(5):1581-
637   97. doi: 10.1016/j.celrep.2018.03.129. PubMed PMID: 29719267; PubMed Central PMCID:
638   PMCPMC5965702.
639   39.   Hooper JE, Feng W, Li H, Leach SM, Phang T, Siska C, et al. Systems biology of facial
640   development: contributions of ectoderm and mesenchyme. Dev Biol. 2017;426(1):97-114. Epub
641   2017/03/29. doi: 10.1016/j.ydbio.2017.03.025. PubMed PMID: 28363736; PubMed Central
642   PMCID: PMCPMC5530582.
643   40.   Diez-Roux G, Banfi S, Sultan M, Geffers L, Anand S, Rozado D, et al. A high-resolution
644   anatomical atlas of the transcriptome in the mouse embryo. PLoS Biol. 2011;9(1):e1000582.
645   Epub 2011/01/18. doi: 10.1371/journal.pbio.1000582. PubMed PMID: 21267068; PubMed
646   Central PMCID: PMCPMC3022534.
647   41.   Mackay TFC, Stone EA, Ayroles JF. The genetics of quantitative traits: challenges and
648   prospects. Nat Rev Genet. 2009;10(8):565-77. doi:
649   http://www.nature.com/nrg/journal/v10/n8/suppinfo/nrg2612_S1.html.
650   42.   Weinberg SM, Roosenboom J, Shaffer JR, Shriver MD, Wysocka J, Claes P. Hunting for
651   genes that shape human faces: Initial successes and challenges for the future. Orthod Craniofac
652   Res. 2019;22 Suppl 1:207-12. doi: 10.1111/ocr.12268. PubMed PMID: 31074157; PubMed
653   Central PMCID: PMCPMC6550302.
654   43.   Svenson KL, Gatti DM, Valdar W, Welsh CE, Cheng R, Chesler EJ, et al. High-resolution
655   genetic mapping using the Mouse Diversity outbred population. Genetics. 2012;190(2):437-47.
656   doi: 10.1534/genetics.111.132597. PubMed PMID: 22345611; PubMed Central PMCID:
657   PMCPMC3276626.
658   44.   Churchill GA, Gatti DM, Munger SC, Svenson KL. The Diversity Outbred mouse
659   population. Mamm Genome. 2012;23(9-10):713-8. Epub 2012/08/15. doi: 10.1007/s00335-012-
660   9414-2. PubMed PMID: 22892839; PubMed Central PMCID: PMCPMC3524832.
661   45.   Chesler EJ, Gatti DM, Morgan AP, Strobel M, Trepanier L, Oberbeck D, et al. Diversity
662   Outbred Mice at 21: Maintaining Allelic Variation in the Face of Selection. G3 (Bethesda).
663   2016;6(12):3893-902. Epub 2016/12/07. doi: 10.1534/g3.116.035527. PubMed PMID:
664   27694113; PubMed Central PMCID: PMCPMC5144960.

665   46.   Yang H, Wang JR, Didion JP, Buus RJ, Bell TA, Welsh CE, et al. Subspecific origin and
666   haplotype diversity in the laboratory mouse. Nat Genet. 2011;43(7):648-55. Epub 2011/05/29.
667   doi: 10.1038/ng.847. PubMed PMID: 21623374; PubMed Central PMCID: PMCPMC3125408.
668   47.   Consortium CC. The genome architecture of the Collaborative Cross mouse genetic
669   reference population. Genetics. 2012;190(2):389-401. doi: 10.1534/genetics.111.132639.
670   PubMed PMID: 22345608; PubMed Central PMCID: PMCPMC3276630.
671   48.   Broman KW, Gatti DM, Simecek P, Furlotte NA, Prins P, Sen Ś, et al. R/qtl2: Software for
672   Mapping Quantitative Trait Loci with High-Dimensional Data and Multiparent Populations.
673   Genetics. 2019;211(2):495-502. Epub 2018/12/27. doi: 10.1534/genetics.118.301595. PubMed
674   PMID: 30591514; PubMed Central PMCID: PMCPMC6366910.
675   49.   Gatti DM, Svenson KL, Shabalin A, Wu LY, Valdar W, Simecek P, et al. Quantitative trait
676   locus mapping methods for diversity outbred mice. G3 (Bethesda). 2014;4(9):1623-33. Epub
677   2014/09/18. doi: 10.1534/g3.114.013748. PubMed PMID: 25237114; PubMed Central PMCID:
678   PMCPMC4169154.
679   50.   Runcie DE, Mukherjee S. Dissecting High-Dimensional Phenotypes with Bayesian Sparse
680   Factor Analysis of Genetic Covariance Matrices. Genetics. 2013;194(3):753-67. doi:
681   10.1534/genetics.113.151217.
682   51.   Lander ES, Botstein D. Mapping mendelian factors underlying quantitative traits using
683   RFLP linkage maps. Genetics. 1989;121(1):185-99. PubMed PMID: 2563713; PubMed Central
684   PMCID: PMCPMC1203601.
685   52.   Listgarten J, Lippert C, Kadie CM, Davidson RI, Eskin E, Heckerman D. Improved linear
686   mixed models for genome-wide association studies. Nat Methods. 2012;9(6):525-6. Epub
687   2012/05/30. doi: 10.1038/nmeth.2037. PubMed PMID: 22669648; PubMed Central PMCID:
688   PMCPMC3597090.
689   53.   Cheng R, Parker CC, Abney M, Palmer AA. Practical considerations regarding the use of
690   genotype and pedigree data to model relatedness in the context of genome-wide association
691   studies. G3 (Bethesda). 2013;3(10):1861-7. Epub 2013/10/03. doi: 10.1534/g3.113.007948.
692   PubMed PMID: 23979941; PubMed Central PMCID: PMCPMC3789811.
693   54.   Yang J, Zaitlen NA, Goddard ME, Visscher PM, Price AL. Advantages and pitfalls in the
694   application of mixed-model association methods. Nat Genet. 2014;46(2):100-6. doi:
695   10.1038/ng.2876. PubMed PMID: 24473328; PubMed Central PMCID: PMCPMC3989144.
696   55.   Tsagkrasoulis D, Hysi P, Spector T, Montana G. Heritability maps of human face
697   morphology through large-scale automated three-dimensional phenotyping. Sci Rep.
698   2017;7:45885. Epub 2017/04/19. doi: 10.1038/srep45885. PubMed PMID: 28422179; PubMed
699   Central PMCID: PMCPMC5395823.
700   56.   Marroig G, Melo DA, Garcia G. Modularity, noise, and natural selection. Evolution.
701   2012;66(5):1506-24.
702   57.   Mrode RA. Linear models for the prediction of animal breeding values. 3rd ed.
703   Oxfordshire, UK: CABI; 2014.
704   58.   Robinson GK. That BLUP is a good thing: the estimation of random effects. Statistical
705   Science. 1991;6(1):15-51. doi: 10.1214/ss/1177011933.
706   59.   Hallgrimsson B, Katz DC, Aponte JD, Larson JE, Devine J, Gonzalez P, et al. Integration
707   and the developmental genetics of allometry. Integrative and Comparative Biology. 2019, in
708   press.

709 60.   Jolicoeur P, Mosimann JE. Size and shape variation in the painted turtle. A principal
710 component analysis. Growth. 1960;24:339-54. PubMed PMID: 13790416.
711 61.   Mitteroecker P, Gunz P, Bernhard M, Schaefer K, Bookstein F. Comparison of cranial
712 ontogenetic trajectories among great apes and humans. Journal of Human Evolution.
713 2004;46(6):679-98. doi: 10.1016/j.jhevol.2004.03.006.
714 62.   Mosimann JE. Size allometry: Size and shape variables with characterizations of the
715 lognormal and generalized gamma distributions. Journal of the American Statistical Association.
716 1970;65:930-45.
717 63.   Cheverud JM. Relationships among ontogenetic, static, and evolutionary allometry. Am J
718 Phys Anthropol. 1982;59(2):139-49. doi: 10.1002/ajpa.1330590204. PubMed PMID: 7149015.
719 64.   Larson JR, Manyama MF, Cole JB, Gonzalez PN, Percival CJ, Liberton DK, et al. Body size
720 and allometric variation in facial shape in children. Am J Phys Anthropol. 2018;165(2):327-42.
721 Epub 2017/11/27. doi: 10.1002/ajpa.23356. PubMed PMID: 29178597; PubMed Central PMCID:
722 PMCPMC5777898.
723 65.   Goios A, Pereira L, Bogue M, Macaulay V, Amorim A. mtDNA phylogeny and evolution of
724 laboratory mouse strains. Genome Res. 2007;17(3):293-8. Epub 2007/02/06. doi:
725 10.1101/gr.5941007. PubMed PMID: 17284675; PubMed Central PMCID: PMCPMC1800920.
726 66.   Logan RW, Robledo RF, Recla JM, Philip VM, Bubier JA, Jay JJ, et al. High-precision
727 genetic mapping of behavioral traits in the diversity outbred mouse population. Genes Brain
728 Behav. 2013;12(4):424-37. Epub 2013/03/20. doi: 10.1111/gbb.12029. PubMed PMID:
729 23433259; PubMed Central PMCID: PMCPMC3709837.
730 67.   French JE, Gatti DM, Morgan DL, Kissling GE, Shockley KR, Knudsen GA, et al. Diversity
731 Outbred Mice Identify Population-Based Exposure Thresholds and Genetic Factors that
732 Influence Benzene-Induced Genotoxicity. Environ Health Perspect. 2015;123(3):237-45. Epub
733 2014/11/06. doi: 10.1289/ehp.1408202. PubMed PMID: 25376053; PubMed Central PMCID:
734 PMCPMC4348743.
735 68.   Smallwood TL, Gatti DM, Quizon P, Weinstock GM, Jung KC, Zhao L, et al. High-
736 resolution genetic mapping in the diversity outbred mouse population identifies Apobec1 as a
737 candidate gene for atherosclerosis. G3 (Bethesda). 2014;4(12):2353-63. Epub 2014/10/23. doi:
738 10.1534/g3.114.014704. PubMed PMID: 25344410; PubMed Central PMCID: PMCPMC4267931.
739 69.   Shorter JR, Huang W, Beak JY, Hua K, Gatti DM, de Villena FP, et al. Quantitative trait
740 mapping in Diversity Outbred mice identifies two genomic regions associated with heart size.
741 Mamm Genome. 2018;29(1-2):80-9. Epub 2017/12/26. doi: 10.1007/s00335-017-9730-7.
742 PubMed PMID: 29279960; PubMed Central PMCID: PMCPMC6340297.
743 70.   Bressler J, Tsai TF, Wu MY, Tsai SF, Ramirez MA, Armstrong D, et al. The SNRPN
744 promoter is not required for genomic imprinting of the Prader-Willi/Angelman domain in mice.
745 Nat Genet. 2001;28(3):232-40. doi: 10.1038/90067. PubMed PMID: 11431693.
746 71.   Albrecht U, Sutcliffe JS, Cattanach BM, Beechey CV, Armstrong D, Eichele G, et al.
747 Imprinted expression of the murine Angelman syndrome gene, Ube3a, in hippocampal and
748 Purkinje neurons. Nat Genet. 1997;17(1):75-8. doi: 10.1038/ng0997-75. PubMed PMID:
749 9288101.
750 72.   Kobayashi S, Kohda T, Ichikawa H, Ogura A, Ohki M, Kaneko-Ishino T, et al. Paternal
751 expression of a novel imprinted gene, Peg12/Frat3, in the mouse 7C region homologous to the

752   Prader-Willi syndrome region. Biochem Biophys Res Commun. 2002;290(1):403-8. doi:
753   10.1006/bbrc.2001.6160. PubMed PMID: 11779183.
754   73.   Morison IM, Ramsay JP, Spencer HG. A census of mammalian imprinting. Trends Genet.
755   2005;21(8):457-65. doi: 10.1016/j.tig.2005.06.008. PubMed PMID: 15990197.
756   74.   Gray TA, Saitoh S, Nicholls RD. An imprinted, mammalian bicistronic transcript encodes
757   two independent proteins. Proc Natl Acad Sci U S A. 1999;96(10):5616-21. doi:
758   10.1073/pnas.96.10.5616. PubMed PMID: 10318933; PubMed Central PMCID: PMCPMC21909.
759   75.   Knoll JH, Nicholls RD, Magenis RE, Graham JM, Lalande M, Latt SA. Angelman and
760   Prader-Willi syndromes share a common chromosome 15 deletion but differ in parental origin
761   of the deletion. Am J Med Genet. 1989;32(2):285-90. doi: 10.1002/ajmg.1320320235. PubMed
762   PMID: 2564739.
763   76.   Mic FA, Molotkov A, Fan X, Cuenca AE, Duester G. RALDH3, a retinaldehyde
764   dehydrogenase that generates retinoic acid, is expressed in the ventral retina, otic vesicle and
765   olfactory pit during mouse development. Mech Dev. 2000;97(1-2):227-30. doi: 10.1016/s0925-
766   4773(00)00434-2. PubMed PMID: 11025231.
767   77.   Visel A, Thaller C, Eichele G. GenePaint.org: an atlas of gene expression patterns in the
768   mouse embryo. Nucleic Acids Res. 2004;32(Database issue):D552-6. doi: 10.1093/nar/gkh029.
769   PubMed PMID: 14681479; PubMed Central PMCID: PMCPMC308763.
770   78.   Martin KM, Metcalfe JC, Kemp PR. Expression of Klf9 and Klf13 in mouse development.
771   Mech Dev. 2001;103(1-2):149-51. doi: 10.1016/s0925-4773(01)00343-4. PubMed PMID:
772   11335124.
773   79.   Yokoyama S, Ito Y, Ueno-Kudoh H, Shimizu H, Uchibe K, Albini S, et al. A systems
774   approach reveals that the myogenesis genome network is regulated by the transcriptional
775   repressor RP58. Dev Cell. 2009;17(6):836-48. doi: 10.1016/j.devcel.2009.10.011. PubMed PMID:
776   20059953; PubMed Central PMCID: PMCPMC3110151.
777   80.   Unda FJ, Pérez-Nanclares G, Le Morvan V, Hernández C, Vilaxa A, De-la-Fuente M, et al.
778   Dynamic assembly of tight junction-associated proteins ZO-1, ZO-2, ZO-3 and occludin during
779   mouse tooth development. Histol Histopathol. 2003;18(1):27-38. doi: 10.14670/HH-18.27.
780   PubMed PMID: 12507281.
781   81.   Yoshida T, Miyoshi J, Takai Y, Thesleff I. Cooperation of nectin-1 and nectin-3 is required
782   for normal ameloblast function and crown shape development in mouse teeth. Dev Dyn.
783   2010;239(10):2558-69. doi: 10.1002/dvdy.22395. PubMed PMID: 21038445.
784   82.   de Koning DJ, Bovenhuis H, van Arendonk JA. On the detection of imprinted quantitative
785   trait loci in experimental crosses of outbred species. Genetics. 2002;161(2):931-8. PubMed
786   PMID: 12072486; PubMed Central PMCID: PMCPMC1462155.
787   83.   Cheverud JM, Hager R, Roseman C, Fawcett G, Wang B, Wolf JB. Genomic imprinting
788   effects on adult body composition in mice. Proc Natl Acad Sci U S A. 2008;105(11):4253-8. Epub
789   2008/03/12. doi: 10.1073/pnas.0706562105. PubMed PMID: 18337500; PubMed Central
790   PMCID: PMCPMC2393747.
791   84.   Leamy LJ, Klingenberg CP, Sherratt E, Wolf JB, Cheverud JM. A search for quantitative
792   trait loci exhibiting imprinting effects on mouse mandible size and shape. Heredity (Edinb).
793   2008;101(6):518-26. Epub 2008/08/06. doi: 10.1038/hdy.2008.79. PubMed PMID: 18685568.

794   85.   Holm VA, Cassidy SB, Butler MG, Hanchett JM, Greenswag LR, Whitman BY, et al.
795   Prader-Willi syndrome: consensus diagnostic criteria. Pediatrics. 1993;91(2):398-402. PubMed
796   PMID: 8424017; PubMed Central PMCID: PMCPMC6714046.
797   86.   Katz DC, Grote MN, Weaver TD. Changes in human skull morphology across the
798   agricultural transition are consistent with softer diets in preindustrial farming groups. Proc Natl
799   Acad Sci U S A. 2017;114(34):9050-5. Epub 2017/07/24. doi: 10.1073/pnas.1702586114.
800   PubMed PMID: 28739900; PubMed Central PMCID: PMCPMC5576786.
801   87.   Liberzon A, Subramanian A, Pinchback R, Thorvaldsdóttir H, Tamayo P, Mesirov JP.
802   Molecular signatures database (MSigDB) 3.0. Bioinformatics. 2011;27(12):1739-40. Epub
803   2011/05/05. doi: 10.1093/bioinformatics/btr260. PubMed PMID: 21546393; PubMed Central
804   PMCID: PMCPMC3106198.
805   88.   Le N, Nagarajan R, Wang JY, Svaren J, LaPash C, Araki T, et al. Nab proteins are essential
806   for peripheral nervous system myelination. Nat Neurosci. 2005;8(7):932-40. PubMed PMID:
807   16136673.
808   89.   Shi C, Sakuma M, Mooroka T, Liscoe A, Gao H, Croce KJ, et al. Down-regulation of the
809   forkhead transcription factor Foxp1 is required for monocyte differentiation and macrophage
810   function. Blood. 2008;112(12):4699-711. Epub 2008/09/17. doi: 10.1182/blood-2008-01-
811   137018. PubMed PMID: 18799727; PubMed Central PMCID: PMCPMC2597137.
812   90.   Zhao H, Zhou W, Yao Z, Wan Y, Cao J, Zhang L, et al. Foxp1/2/4 regulate endochondral
813   ossification as a suppresser complex. Dev Biol. 2015;398(2):242-54. Epub 2014/12/17. doi:
814   10.1016/j.ydbio.2014.12.007. PubMed PMID: 25527076; PubMed Central PMCID:
815   PMCPMC4342236.
816   91.   Pacheco-Costa R, Kadakia JR, Atkinson EG, Wallace JM, Plotkin LI, Reginato RD.
817   Connexin37 deficiency alters organic bone matrix, cortical bone geometry, and increases
818   Wnt/β-catenin signaling. Bone. 2017;97:105-13. Epub 2017/01/16. doi:
819   10.1016/j.bone.2017.01.010. PubMed PMID: 28096061.
820   92.   Wilson DG, Phamluong K, Lin WY, Barck K, Carano RA, Diehl L, et al. Chondroitin sulfate
821   synthase 1 (Chsy1) is required for bone development and digit patterning. Dev Biol.
822   2012;363(2):413-25. Epub 2012/01/17. doi: 10.1016/j.ydbio.2012.01.005. PubMed PMID:
823   22280990.
824   93.   Xing WR, Goodluck H, Zeng C, Mohan S. Role and mechanism of action of leucine-rich
825   repeat kinase 1 in bone. Bone Res. 2017;5:17003. Epub 2017/03/14. doi:
826   10.1038/boneres.2017.3. PubMed PMID: 28326224; PubMed Central PMCID:
827   PMCPMC5348726.
828   94.   Vecchione L, Byron C, Cooper GM, Barbano T, Hamrick MW, Sciote JJ, et al. Craniofacial
829   morphology in myostatin-deficient mice. J Dent Res. 2007;86(11):1068-72. doi:
830   10.1177/154405910708601109. PubMed PMID: 17959898.
831   95.   Vecchione L, Miller J, Byron C, Cooper GM, Barbano T, Cray J, et al. Age-related changes
832   in craniofacial morphology in GDF-8 (myostatin)-deficient mice. Anat Rec (Hoboken).
833   2010;293(1):32-41. doi: 10.1002/ar.21024. PubMed PMID: 19899116; PubMed Central PMCID:
834   PMCPMC3113544.
835   96.   Sahni M, Ambrosetti DC, Mansukhani A, Gertner R, Levy D, Basilico C. FGF signaling
836   inhibits chondrocyte proliferation and regulates bone development through the STAT-1
837   pathway. Genes & Development. 1999;13:1361-6.

838 97.   Xiao L, Naganawa T, Obugunde E, Gronowicz G, Ornitz DM, Coffin JD, et al. Stat1
839 controls postnatal bone formation by regulating fibroblast growth factor signaling in
840 osteoblasts. J Biol Chem. 2004;279(26):27743-52. Epub 2004/04/08. doi:
841 10.1074/jbc.M314323200. PubMed PMID: 15073186.
842 98.   Kim S, Koga T, Isobe M, Kern BE, Yokochi T, Chin YE, et al. Stat1 functions as a
843 cytoplasmic attenuator of Runx2 in the transcriptional program of osteoblast differentiation.
844 Genes Dev. 2003;17(16):1979-91. doi: 10.1101/gad.1119303. PubMed PMID: 12923053;
845 PubMed Central PMCID: PMCPMC196253.
846 99.   Le Fevre AK, Taylor S, Malek NH, Horn D, Carr CW, Abdul-Rahman OA, et al. FOXP1
847 mutations cause intellectual disability and a recognizable phenotype. Am J Med Genet A.
848 2013;161A(12):3166-75. Epub 2013/09/24. doi: 10.1002/ajmg.a.36174. PubMed PMID:
849 24214399.
850 100.   Tian J, Ling L, Shboul M, Lee H, O'Connor B, Merriman B, et al. Loss of CHSY1, a secreted
851 FRINGE enzyme, causes syndromic brachydactyly in humans via increased NOTCH signaling. Am
852 J Hum Genet. 2010;87(6):768-78. doi: 10.1016/j.ajhg.2010.11.005. PubMed PMID: 21129727;
853 PubMed Central PMCID: PMCPMC2997365.
854 101.   Huh A, Horton MJ, Cuenco KT, Raoul G, Rowlerson AM, Ferri J, et al. Epigenetic influence
855 of KAT6B and HDAC4 in the development of skeletal malocclusion. Am J Orthod Dentofacial
856 Orthop. 2013;144(4):568-76. doi: 10.1016/j.ajodo.2013.06.016. PubMed PMID: 24075665;
857 PubMed Central PMCID: PMCPMC3849704.
858 102.   Vimalraj S, Arumugam B, Miranda PJ, Selvamurugan N. Runx2: Structure, function, and
859 phosphorylation in osteoblast differentiation. Int J Biol Macromol. 2015;78:202-8. Epub
860 2015/04/13. doi: 10.1016/j.ijbiomac.2015.04.008. PubMed PMID: 25881954.
861 103.   Clayton-Smith J, O'Sullivan J, Daly S, Bhaskar S, Day R, Anderson B, et al. Whole-exome-
862 sequencing identifies mutations in histone acetyltransferase gene KAT6B in individuals with the
863 Say-Barber-Biesecker variant of Ohdo syndrome. Am J Hum Genet. 2011;89(5):675-81. doi:
864 10.1016/j.ajhg.2011.10.008. PubMed PMID: 22077973; PubMed Central PMCID:
865 PMCPMC3213399.
866 104.   Sena K, Morotome Y, Baba O, Terashima T, Takano Y, Ishikawa I. Gene expression of
867 growth differentiation factors in the developing periodontium of rat molars. J Dent Res.
868 2003;82(3):166-71. doi: 10.1177/154405910308200304. PubMed PMID: 12598543.
869 105.   Nakashima M, Toyono T, Murakami T, Akamine A. Transforming growth factor-beta
870 superfamily members expressed in rat incisor pulp. Arch Oral Biol. 1998;43(9):745-51. doi:
871 10.1016/s0003-9969(98)00046-6. PubMed PMID: 9783830.
872 106.   Cerny R, Cattell M, Sauka-Spengler T, Bronner-Fraser M, Yu F, Medeiros DM. Evidence
873 for the prepattern/cooption model of vertebrate jaw evolution. Proc Natl Acad Sci U S A.
874 2010;107(40):17262-7. Epub 2010/09/20. doi: 10.1073/pnas.1009304107. PubMed PMID:
875 20855630; PubMed Central PMCID: PMCPMC2951391.
876 107.   So PL, Danielian PS. Cloning and expression analysis of a mouse gene related to
877 Drosophila odd-skipped. Mech Dev. 1999;84(1-2):157-60. PubMed PMID: 10473132.
878 108.   Kawai S, Yamauchi M, Amano A. Zinc-finger transcription factor Odd-skipped related 1
879 regulates cranial bone formation. J Bone Miner Metab. 2018;36(6):640-7. Epub 2017/12/12.
880 doi: 10.1007/s00774-017-0885-9. PubMed PMID: 29234951.

881   109.   Jeong J, Cesario J, Zhao Y, Burns L, Westphal H, Rubenstein JL. Cleft palate defect of
882   Dlx1/2-/- mutant mice is caused by lack of vertical outgrowth in the posterior palate. Dev Dyn.
883   2012;241(11):1757-69. Epub 2012/09/28. doi: 10.1002/dvdy.23867. PubMed PMID: 22972697;
884   PubMed Central PMCID: PMCPMC3988582.
885   110.   Zelzer E, McLean W, Ng YS, Fukai N, Reginato AM, Lovejoy S, et al. Skeletal defects in
886   VEGF(120/120) mice reveal multiple roles for VEGF in skeletogenesis. Development.
887   2002;129(8):1893-904. PubMed PMID: 11934855.
888   111.   R Development Core Team. R: A language and environment for statistical computing. R
889   Foundation for Statistical Computing, Vienna, Austria. URL http://www.R-project.org/2015.
890   112.   Mitteroecker P, Gunz P. Advances in Geometric Morphometrics. Evolutionary Biology.
891   2009;36(2):235-47. doi: 10.1007/s11692-009-9055-x.
892   113.   Schlager S. Morpho and Rvcg – Shape Analysis in R. In: Zheng G, Li S, Szekely G, editors.
893   Statistical Shape and Deformation Analysis: Academic Press; 2017. p. 217-56.
894   114.   Mardia KV, Bookstein FL, Moreton IJ. Statistical assessment of bilateral symmetry of
895   shapes. Biometrika. 2000;87(2):285-300.
896   115.   Klingenberg CP, Barluenga M, Meyer A. Shape analysis of symmetric structures:
897   quantifying variation among individuals and asymmetry. Evolution. 2002;56(10):1909-20.
898   PubMed PMID: 12449478.
899   116.   Morgan AP, Fu CP, Kao CY, Welsh CE, Didion JP, Yadgary L, et al. The Mouse Universal
900   Genotyping Array: From Substrains to Subspecies. G3 (Bethesda). 2015;6(2):263-79. Epub
901   2015/12/18. doi: 10.1534/g3.115.022087. PubMed PMID: 26684931; PubMed Central PMCID:
902   PMCPMC4751547.
903   117.   Didion JP, Morgan AP, Clayshulte AM, Mcmullan RC, Yadgary L, Petkov PM, et al. A
904   multi-megabase copy number gain causes maternal transmission ratio distortion on mouse
905   chromosome 2. PLoS Genet. 2015;11(2):e1004850. Epub 2015/02/13. doi:
906   10.1371/journal.pgen.1004850. PubMed PMID: 25679959; PubMed Central PMCID:
907   PMCPMC4334553.
908   118.   Cardon LR, Palmer LJ. Population stratification and spurious allelic association. Lancet.
909   2003;361(9357):598-604. doi: 10.1016/S0140-6736(03)12520-2. PubMed PMID: 12598158.
910   119.   Broman KW, Gatti DM, Svenson KL, Sen Ś, Churchill GA. Cleaning Genotype Data from
911   Diversity Outbred Mice. G3 (Bethesda). 2019;9(5):1571-9. Epub 2019/05/07. doi:
912   10.1534/g3.119.400165. PubMed PMID: 30877082; PubMed Central PMCID: PMCPMC6505173.
913   120.   Sybert VP, McCauley E. Turner's syndrome. N Engl J Med. 2004;351(12):1227-38. doi:
914   10.1056/NEJMra030360. PubMed PMID: 15371580.
915   121.   Hallgrimsson BA, J David, Katz DC, Bannister JJ, Riccardi SL, Mahasuwan N, McInnes BL,
916   et al. Automated syndrome diagnosis by three-dimensional facial photogrammetric imaging.
917   American Journal of Human Genetics. 2019, in review.
918   122.   Krzanowski WJ. Principles of Multivariate Analysis: A User's Perspective. New York:
919   Oxford University Press; 2005.
920   123.   Churchill GA, Doerge RW. Empirical threshold values for quantitative trait mapping.
921   Genetics. 1994;138(3):963-71. PubMed PMID: 7851788; PubMed Central PMCID:
922   PMCPMC1206241.
923   124.   Manichaikul A, Dupuis J, Sen S, Broman KW. Poor performance of bootstrap confidence
924   intervals for the location of a quantitative trait locus. Genetics. 2006;174(1):481-9. Epub

925   2006/06/18. doi: 10.1534/genetics.106.061549. PubMed PMID: 16783000; PubMed Central
926   PMCID: PMCPMC1569776.
927   125.   Yalcin B, Flint J, Mott R. Using progenitor strain information to identify quantitative trait
928   nucleotides in outbred mice. Genetics. 2005;171(2):673-81. Epub 2005/08/05. doi:
929   10.1534/genetics.104.028902. PubMed PMID: 16085706; PubMed Central PMCID:
930   PMCPMC1456780.
931   126.   Baud A, Hermsen R, Guryev V, Stridh P, Graham D, McBride MW, et al. Combined
932   sequence-based and genetic mapping analysis of complex traits in outbred rats. Nat Genet.
933   2013;45(7):767-75. Epub 2013/05/26. doi: 10.1038/ng.2644. PubMed PMID: 23708188;
934   PubMed Central PMCID: PMCPMC3821058.
935   127.   Rhee SY, Wood V, Dolinski K, Draghici S. Use and misuse of the gene ontology
936   annotations. Nat Rev Genet. 2008;9(7):509-15. Epub 2008/05/13. doi: 10.1038/nrg2363.
937   PubMed PMID: 18475267.
938   128.   Maglott D, Ostell J, Pruitt KD, Tatusova T. Entrez Gene: gene-centered information at
939   NCBI. Nucleic Acids Res. 2011;39(Database issue):D52-7. Epub 2010/11/28. doi:
940   10.1093/nar/gkq1237. PubMed PMID: 21115458; PubMed Central PMCID: PMCPMC3013746.
941   129.   Subramanian A, Tamayo P, Mootha VK, Mukherjee S, Ebert BL, Gillette MA, et al. Gene
942   set enrichment analysis: a knowledge-based approach for interpreting genome-wide expression
943   profiles. Proc Natl Acad Sci U S A. 2005;102(43):15545-50. Epub 2005/09/30. doi:
944   10.1073/pnas.0506580102. PubMed PMID: 16199517; PubMed Central PMCID:
945   PMCPMC1239896.
946   130.   Katz DC, Grote MN, Weaver TD. A mixed model for the relationship between climate
947   and cranial form. American Journal of Physical Anthropology. 2016;160:593-603.
948   131.   Mitteroecker P, Cheverud JM, Pavlicev M. Multivariate Analysis of Genotype-Phenotype
949   Association. Genetics. 2016. doi: 10.1534/genetics.115.181339.
950   132.   Nakagawa S, Schielzeth H. A general and simple method for obtaining R^2 from
951   generalized linear mixed-effects models. Methods in Ecology and Evolution. 2013;4:133-42. doi:
952   10.1111/j.2041-210x.2012.00261.x.
953   133.   Adler D, Murdoch D, others. rgl: 3D Visualization Using OpenGL. 0.95.1441 ed2016.
954   134.   Rohlf FJ. Shape statistics: Procrustes superimpositions and tangent spaces. Journal of
955   Classification. 1999;16(2):197-223.
956

Supporting Information

S1 Fig. Eigenvalue decay. Percentage of total variation explained for each shape principal

component. We performed genome scans for all PCs explaining more than 1% of shape

variation (red point identifies cutoff at PC 20) and subjected the first five PCs (green point

identifies PC 5 floor) to in-depth analysis.

962   **S2 Fig. Change in chromosome 2 WSB allele frequencies over generations.** Sample-wide WSB

963   allele frequency on chromosome 2 by DO generation. The high WSB allele frequency in earlier

964   generations reflects meiotic drive for WSB at the *R2d2* locus. Declining frequencies in later

965   generations reflect the systematic purge of WSB alleles from the DO population.

966   **S1 Table.** LOD peaks and support intervals for all QTL on PCs 1-20.

967   **S2 Table.** Full array of LOCO mean heritabilities over PCs 1-20.

968   **S1 File. Genes, PCs 1-5.** All named, protein-coding genes in the PC 1-5 QTL intervals.

969   **S2 File. Top GO annotations, PCs 1-5.** Top 100 FDR q-value GO terms for the PC 1-5 QTL interval

970   gene set (Molecular Signatures Database output file).

971   **S3 File. Top GO annotations, PC 1.** For the PC1 QTL interval gene set, GO terms with FDR q-

972   value < 0.05 (Molecular Signatures Database output file).

973